Surface Science Studies of the Photoactivation of TiO_2—New Photochemical Processes

Tracy L.Thompson and John T. Yates, Jr.*

Surface Science Center, Department of Chemistry, University of Pittsburgh, 219 Parkman Avenue, Pittsburgh, Pennsylvania 15260

Received January 11, 2006

Contents

* Corresponding author [e-mail jyates@pitt.edu; telephone (412) 624-8320; fax (412) 624-6003].

1. Introduction

The photoactivation of TiO_2 has received enormous attention from scientists and engineers in the past decade. This interest has been generated because of the confluence of several extraordinary developments: (1) the major success of the Grätzel solar cell,[1−3] employing TiO_2 as the active semiconductor, in which TiO_2 has been modified to enhance its efficiency in producing electrical energy; (2) the use of TiO_2 as a medium for environmental cleanup through activation of the photo-oxidation of organic pollutants on self-cleaning surfaces, work that has been stimulated by many Japanese workers, leading to a revolution in Japan now spreading westward through a wide variety of TiO_2-based technological innovations,[4] in addition to much work from Europe and the United States that has contributed to the accelerating interest in TiO_2-based photochemistry; (3) the development of hydrophilic surfaces activated by solar energy;[5,6] and (4) the recent discovery that TiO_2-based self-cleaning surfaces also exhibit antimicrobial activity useful in the home and in the hospital.[4,7]

During the period encompassing these technological developments, the pace of scientific research on the photochemistry on TiO_2 surfaces has doubled and redoubled in periods of about 5 years as may be seen from the survey shown in Figure 1.

This review encompasses several scientific themes that underpin our increasing understanding of TiO_2 as a photoactive semiconducting material. The review builds upon an earlier review titled "Photocatalysis on TiO_2 Surfaces—Principles, Mechanisms, and Selected Results",[8] which is now 11 years old. In the current review, topics of particular concern are (1) the role of both surface and bulk defects and bulk impurities in influencing the photosensitivity of TiO_2; (2) the recombination of charge carriers in TiO_2; (3) the transfer of charge from photoexcited TiO_2 to molecules bound to the TiO_2 surface; (4) new insights into the photoexcitation of TiO_2 afforded by detailed studies of the photodesorption of chemisorbed O_2; and (5) the origin of the photoinduced hydrophilicity of TiO_2. These five topics represent areas of our current research where an element of coherence in understanding exists as a result of the work of many others on similar basic issues. Primarily, experiments involving the use of surface science methods are included because it is through the tight control and careful measurement of surface properties that insight into fundamentals governing photochemistry on TiO_2 surfaces may be gained with some certainty. Because of the large volume of papers dealing with photochemistry on TiO_2, as shown by Figure 1, it is not possible for this review to be fully comprehensive. Some studies of more poorly defined powdered TiO_2 surfaces

10.1021/cr050172k CCC: $59.00
Published on Web 10/11/2006

Tracy L. Thompson was born on January 8, 1979, in Cleveland, OH. Tracy received her bachelor's of science from Baldwin-Wallace College in 2000 and her Ph.D. in physical chemistry from the University of Pittsburgh under the direction of John T. Yates, Jr., in January 2006. Tracy's dissertation research focused on photochemical and photophysical measurements of titanium dioxide single crystals using ultrahigh vacuum techniques. Research was completed in the areas of chemical doping of TiO_2 surfaces, photodecomposition of organic pollutants over TiO_2 surfaces, and kinetic investigations of the interaction of TiO_2 surfaces with UV light. During her graduate career, Tracy has authored or co-authored more than 14 peer-reviewed publications, including 2 review articles. Tracy is currently employed at Graftech International Ltd., a carbon and graphite materials science company headquartered in Cleveland, OH.

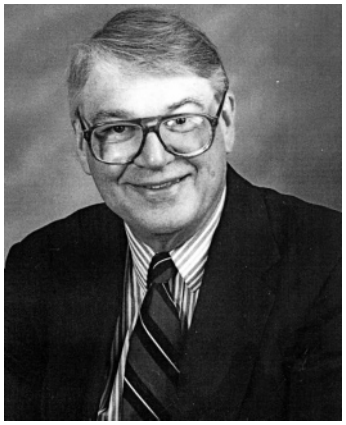

Professor Yates holds the R. K. Mellon Chair in the Department of Chemistry and Department of Physics and Astronomy at the University of Pittsburgh. He is the founder (1982) and current Director of the Surface Science Center. He received his B.S. degree from Juniata College and his Ph.D. from MIT. He is a member of the National Academy of Sciences. His research interests in many areas of surface chemistry and physics are reported in more than 600 publications and result from the mentoring of more than 40 Ph.D. students. In October 2006, he will join the Chemistry Department at the University of Virginia.

are also reported, especially when there is a conceptual connection to the surface science work done on single-crystal substrates. Numerous surface studies of TiO_2 at the atomic level of detail attest to the additional complexity of compound semiconductor surfaces compared to metals or elemental semiconductors.

2. Properties of TiO_2 Materials

Other comprehensive reviews dealing with the structure of TiO_2 materials exist.[9,10] A brief synopsis will be presented here to facilitate a more complete understanding of the following sections in this review.

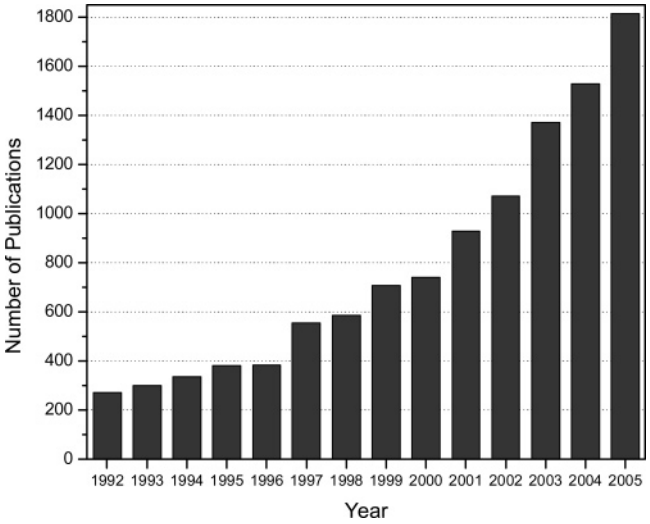

Figure 1. Annual number of papers published in which "TiO_2 or titanium dioxide" and "photo-" are mentioned, beginning in 1992 through November 2005. Literature search was done using ISI's Web of Science (www.isiknowledge.com).

2.1. Bulk Structure

Titanium dioxide can exist in one of three bulk crystalline forms: rutile, anatase, and brookite. Diebold[9] has reviewed the basic structural characteristics of both anatase and rutile materials; the brookite structure is not often used for experimental investigations. In addition, Henrich and Cox[11] present a generalized discussion of the bulk structures of many metal oxide crystals. Both the rutile and anatase crystal structures are in distorted octahedron classes.[12] In rutile, slight distortion from orthorhombic structure occurs, where the unit cell is stretched beyond a cubic shape. In anatase, the distortion of the cubic lattice is more significant, and thus the resulting symmetry is less orthorhombic. Figure 2 depicts the distorted octahedral symmetries characteristic of rutile (left) and anatase (right).

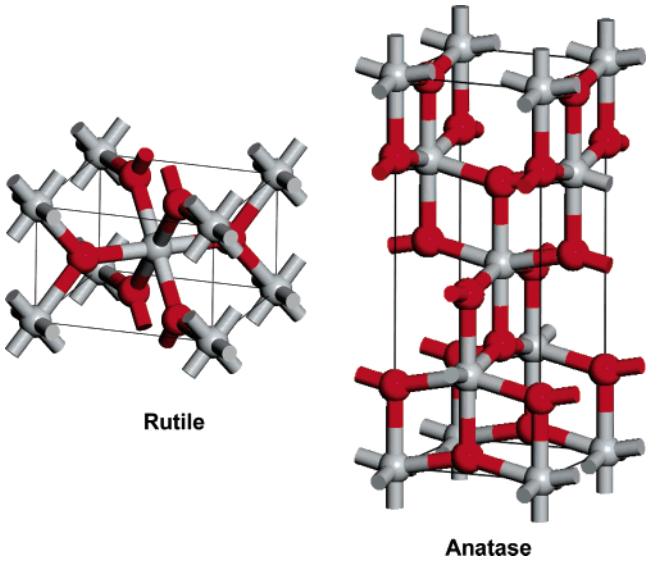

Figure 2. Bulk crystal structure of rutile (left) and anatase (right). Titanium atoms are gray, and oxygen atoms are red.

2.2. Surface Structure of TiO_2(110)

Most of the surface science studies of photochemistry on TiO_2 have been concerned with the rutile single-crystal surface. Anatase single crystals are very difficult to obtain,

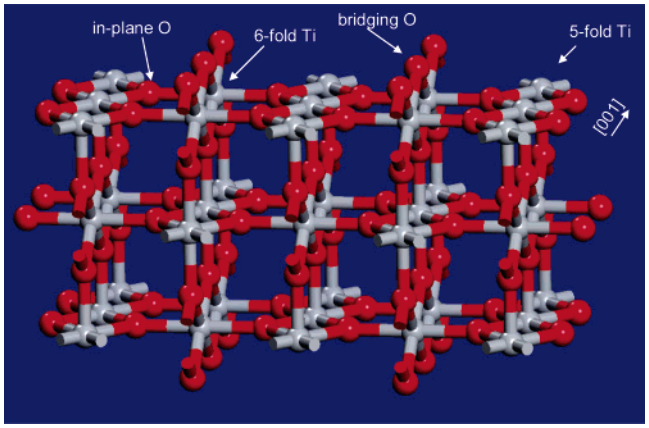

Figure 3. Surface structure of the stoichiometric $TiO_2(110)-(1 \times 1)$ surface depicting the two different types of surface titanium and oxygen atoms present.

and only a few surface science investigations of anatase are available. It is reported that anatase is more active photocatalytically. Also, technological uses of TiO_2 often employ colloidal TiO_2 particles in thin films, and these preparations may contain a high fraction of anatase particles. It remains to be seen whether the large number of well-controlled studies on rutile surfaces will provide key information useful in technology when anatase surfaces are involved. The surface structure of the rutile $TiO_2(110)$ surface has been well characterized, as it is the most commonly investigated titania crystal face. The surface consists of rows of bridging oxygen atoms that lie above the in-plane surface. The rows of bridging oxygen atoms are located directly on top of 6-fold coordinated Ti rows. The 6-fold coordinated Ti rows exist in the same plane as 5-fold coordinated Ti atoms. The rows of 5- and 6-fold Ti atoms are separated by rows of in-plane oxygen atoms. A model of the stoichiometric surface depicting all four types of surface atoms is shown in Figure 3.

The detailed structure of the $TiO_2(110)$ surface has been investigated by ab initio theoretical methods,[13] by surface X-ray diffraction (SXRD),[14] and very recently by low-energy electron diffraction.[15] The surface O atoms and the surface Ti atoms are expected to be in distorted positions relative to the bulk. The extent of the lattice relaxation measured by SXRD and calculated theoretically differs by about 0.3 Å (O) and 0.1 Å (Ti). Recent LEED I/V measurements and analysis involving adjustable self-consistent phase shifts[15] have eliminated this discrepancy and show that an O atom outward relaxation of about 0.1 Å occurs, accompanied by an outward Ti atom relaxation of about 0.25 Å.[15]

2.2.1. Measuring Defects: $TiO_2(110)-(1 \times 1)$

The photoactivity of the $TiO_2(110)$ surface is critically dependent on the presence of defects in the surface region of the crystal substrate. These defects, known to be oxygen vacancies located in the bridging oxygen rows, can be created by thermal annealing[9,16,17] or by ion sputtering[18] and have been previously quantified using He ion scattering[19,20] and scanning tunneling microscopy,[9,21,22] as well as by XPS,[18,20,23−25] UPS,[24] EELS,[25] and EPR spectroscopy.[26−28] The presence of these defects changes the electronic structure of the material. It is currently not known whether defect sites influence the efficiency of the electronic excitation of TiO_2 or the efficiency of charge transfer to adsorbates. It is likely that electron−hole recombination processes are influenced

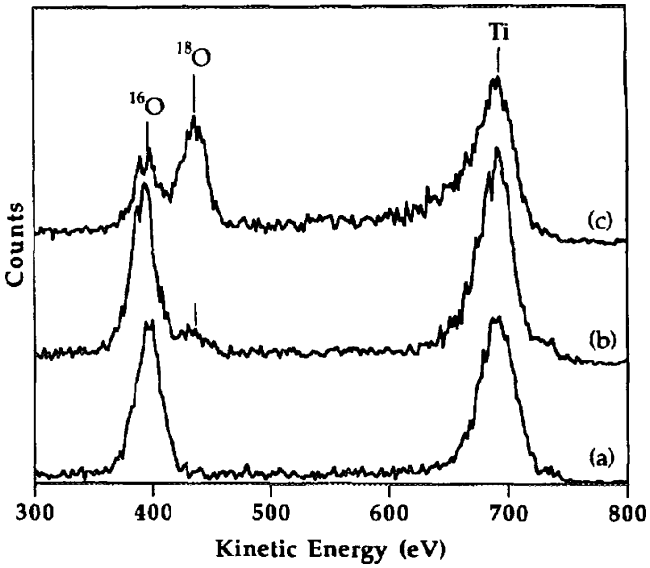

Figure 4. Low-energy ion scattering spectra following $^{18}O_2$ adsorption on three differently treated $TiO_2(110)$ surfaces: (a) stoichiometric surface, containing few defects; (b) slightly oxygen deficient surface; (c) highly defective surface. Reprinted with permission from ref 20. Copyright 1992 AVS The Science and Technology Society,

by defect sites (see section 5.1.1), causing an enhancement in chemical rates which depend on charge transfer from either electrons or holes. It is known that adsorbed molecules are often bound to surface defects where charge transfer can occur to these proximate surface species.

Data illustrating the use of low-energy He ion spectroscopy (LEIS) are presented in Figure 4. Here, 1 keV He^+ ions are directed in a beam to the TiO_2 surface. Momentum transfer occurs to individual atoms in the surface, and the law of conservation of momentum is used to determine the mass of the surface atom participating in a collision, through measurement of the kinetic energy of the reflected He^+ ion originating from the collision. The fully oxidized $TiO_2(110)$ crystal (1×1 LEED pattern) was made slightly defective by annealing the surface for 3 min in ultrahigh vacuum at 1000 K. Then, $^{18}O_2$ was adsorbed on the surface, localizing on the defect sites and labeling them with the isotopic oxygen. The LEIS measurements show that the nondefective surface consisting of known numbers of Ti and ^{16}O atoms exhibits kinetic energies characteristic of ^{16}O and Ti in spectrum a. When the slightly defective surface is studied, containing ^{18}O on the defect sites, spectrum b is obtained, and from the area of the ^{18}O feature it was determined that ~0.07 ML of defects containing the ^{18}O label were present. Spectrum c was obtained when a highly defective surface, sputtered with 500 eV Ar^+ ions at a fluence of 2×10^{16} ions/cm^2, was similarly studied. In parallel XPS studies, the slightly defective $TiO_2(110)$ surface was shown to exhibit a weak feature due to small amounts of Ti^{3+} present when the surface defects were produced by heating to 1000 K.[20] Further structural characterization of the defective TiO_2 surface, as well as the induced electronic changes associated with defect sites, is discussed thoroughly by Diebold.[9]

It has been found that STM images of oxygen defects may be influenced by the dissociation of traces of water vapor present in ultrahigh-vacuum systems, causing the defect to adsorb a hydroxyl group. This finding is completely consistent with other earlier studies of the interaction of oxygen vacancy defect sites to produce water dissociation and surface

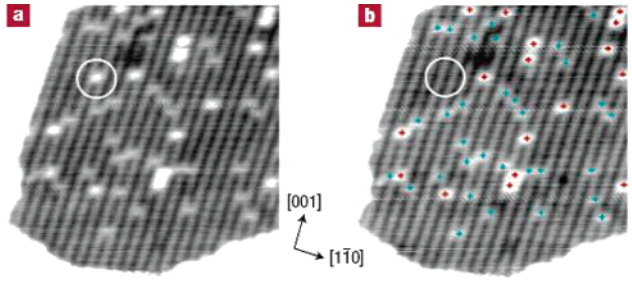

Figure 5. STM studies of partially hydroxylated TiO_2(110) containing some nonhydroxylated oxygen vacancy defects: (a) before voltage pulse; (b) after voltage pulse. The red and blue crosses mark hydroxylated and nonhydroxylated defect sites, respectively, and the circled site shows the conversion of a hydroxyl group by an electron pulse to an O-filled site as the OH group is decomposed. Scale = 15 nm × 15 nm. Reprinted with permission from ref 32. Copyright 2006 Macmillan Publishers Ltd.

hydroxyl groups.[29−31] Although both the defect and the hydroxyl group are bright by STM, the hydroxyl group is brighter than the defect.[32,33] This has caused a reinterpretation of earlier work[34,35] to be necessary, in which the role of hydroxyl groups was not recognized. A clear distinction between the defect STM images and the hydroxylated defect images has been correctly recognized by Thornton et al.,[32] who have additionally shown that the hydroxylated defects may be converted to nonhydroxylated sites using electron pulses from the STM tip. Figure 5a shows an STM image of a TiO_2(110) surface containing vacancy defects (the bright points with the lowest brightness) mixed with other sites that give the brightest images. The bright points with the lower brightness are true oxygen-vacancy defects, whereas the brighter image points are hydroxyl groups, made from residual water dissociation on the vacancy defects. These two types of sites are marked with blue and red dots, respectively, in Figure 5b. A (3 V, 0.35 nA, 300 ms) pulse from the STM tip was applied to a hydroxyl group circled in Figure 5a, and it was observed that this treatment caused it to convert to a nondefective dark site as may be seen by comparing the circled regions in panels a and b of Figure 5. This experiment demonstrates that water molecules dissociate at O-vacancy sites and that when the H atoms are removed from the formed −OH groups, the O atom remains behind, healing the vacancy defect site.[32]

The coverage of surface defects that are created by thermal annealing can be analyzed through the adsorption and subsequent thermal desorption of CO_2 from the TiO_2(110) surface.[16,30] On the stoichiometric TiO_2(110) surface, CO_2 adsorbs at regular Ti^{4+} sites on the surface of the crystal (E_{des} = 48.5 kJ mol^{-1}). The coverage-dependent thermal desorption spectra for CO_2 adsorbed at these sites consists of a single peak near 160 K. Upon annealing to temperatures near 600 K, defect formation on the TiO_2(110)−(1 × 1) surface begins to occur and these defective surfaces are often called reduced surfaces. The presence of defects on the partially reduced surface can be detected using CO_2 as a probe molecule: CO_2 preferentially adsorbs on defect sites at low coverages.[30] At higher coverage, when defects are present, CO_2 adsorbs on both defect sites (E_{des} = 54.0 kJ mol^{-1}) and on regular sites. The thermal desorption profile for CO_2 from TiO_2(110) consists of a two-peak pattern characteristic of the quantity of defects present as the annealing temperature is increased. A comparison of the thermal desorption spectra for CO_2 from an oxidized TiO_2(110) surface to the same for a reduced TiO_2(110) surface is shown in Figure 6. This method serves as a simple quantitative measure of the surface defect density on TiO_2(110) single-crystalline substrates.

Various quantitative studies of the coverage of defects versus annealing temperature show that the defect coverage reaches a maximum of about 10% of a monolayer when the TiO_2(110) surface is heated to ∼900 K.[20] This value is maintained even with additional heating due to the diffusion of titanium interstitial atoms from the surface region of the crystal to regions deeper within the bulk of the TiO_2.[36,37] This process establishes an equilibrium concentration of oxygen vacancies that is maintained even with extensive annealing at temperatures at or below 900 K as described by Henderson.[36,37] There are various possible models that could be postulated to explain the maintenance of a constant defect level on the surface of TiO_2(110) after long heating. Figure 7 shows two models schematically. In model 1, O vacancies in the surface region diffuse into the bulk, being replaced by O^{2-} anions from the bulk. In model 2, reduced Ti cation (Ti^{3+}) species diffuse into the bulk during long heating. Either model could produce a steady-state level of defects in the surface region. In the literature prior to the work of ref 36, the O-vacancy diffusion model has been preferred. Using static secondary mass spectroscopy (SSIMS), in which surface ionization by 3 keV of Ar^+ ions is carried out at very low ion fluxes, both $^{48}Ti^+$ ions and $^{48}TiO^+$ ions

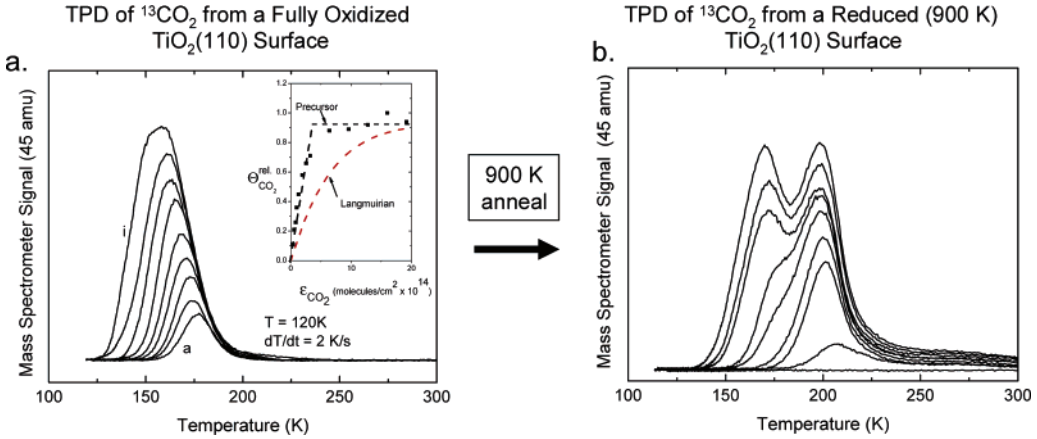

Figure 6. Comparison of the thermal desorption spectra for CO_2 from an oxidized stoichiometric surface to the CO_2 desorption from a reduced (900 K, 1 h) surface. CO_2 preferentially adsorbs at defect sites on the reduced surface. The inset in (a) shows the coverage (θ) versus exposure (ϵ) data for CO_2 adsorbed on the oxidized surface: a mobile precursor mechanism describes the adsorption process. Reprinted with permission from ref 16. Copyright 2003 American Chemical Society.

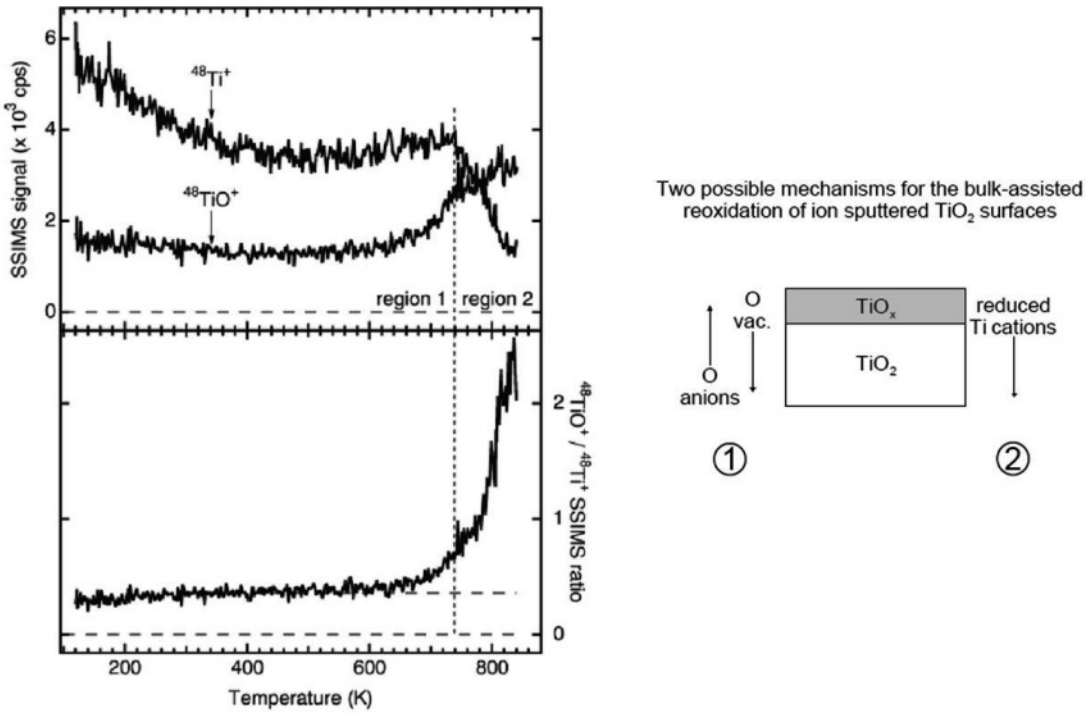

Figure 7. Temperature-programmed static secondary ion mass spectroscopy study of the behavior of TiO_2(110) as it is heated in vacuum. On the left, the upper traces show ions characteristic of Ti^{3+} surface species and Ti^{4+} species, illustrating the inward migration of Ti^{3+} accompanied by the outward migration of Ti^{4+}. The bottom panel on the left shows the ratio of the ion signals during annealing. The panel on the right shows two models for the removal of Ti^{3+} from the surface during annealing, and the data indicate that model 2 is obeyed. Reprinted with permission from ref 36. Copyright 1999 Elsevier B.V.

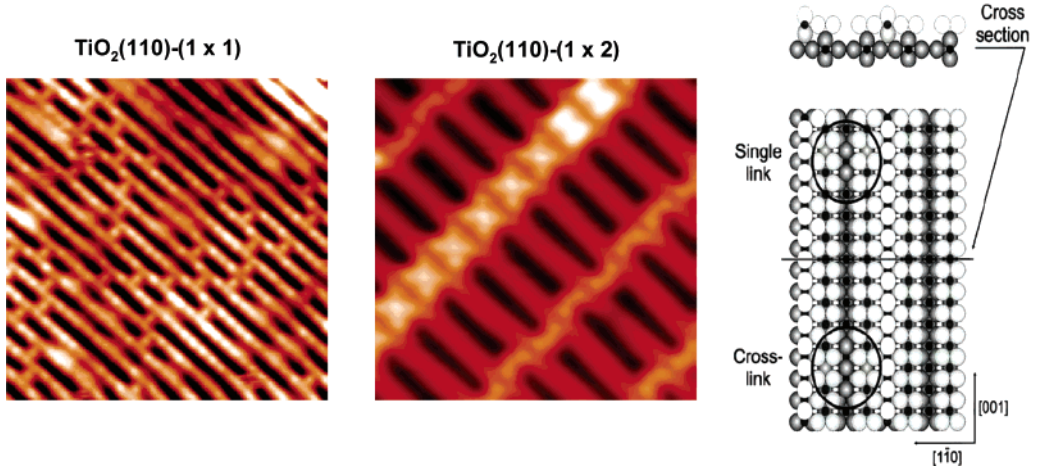

Figure 8. STM images of the reduced TiO_2(110)−(1 × 1) surface (left) and the extensively reduced TiO_2(110)−(1 × 2) surface (right). The (1 × 2) surface reconstruction forms after extensive annealing at temperatures near 1100 K. The (1 × 2) surface exhibits both single-link and cross-link features, shown schematically in the ball model on the right-hand side of the figure. Reprinted with permission from ref 41. Copyright 2003 Elsevier B.V.

were monitored as a function of the annealing temperature of a TiO_2(110) surface, which had been heavily damaged by extensive Ar^+ ion bombardment producing many defects, such as shown previously in the LEIS measurements (Figure 4b). The behaviors of the $^{48}Ti^+$ signal and the $^{48}TiO^+$ signal are shown in the top panel of Figure 7. In the bottom panel, the ratio $^{48}TiO^+/^{48}Ti^+$ is thought to be indicative of the inward migration of reduced cations (Ti^{3+}) during heating, supporting model 2 in Figure 7. These Ti^{3+} ions produce $^{48}Ti^+$ ions in the SSIMS process. More detailed studies support this conclusion that Ti^{3+} migration into the bulk is responsible for the steady-state concentration of surface vacancy defects produced on TiO_2(110) upon long heating.[36]

2.2.2. Extensive Defect Formation: TiO_2(110)–(1 × 2)

With more extensive annealing above ~1100 K, a (1 × 2) reconstruction of the TiO_2(110) surface occurs. The conversion between the slightly defective surface (1 × 1) and the (1 × 2) reconstruction is seen in Figure 8. The (1 × 2) surface consists of a cross-link structure as well as a single-link structure. On the right side of Figure 8, a diagram of the cross-link and single-link features is presented and has been described by Stone et al.[38] The atomic nature of the (1 × 2) surface structure has been debated in the past. For a detailed overview of the (1 × 2) surface reconstruction and the models presented to describe this surface, the authors

refer the reader to ref 9, which includes references to the majority of research done on this surface. Since the publication of ref 9, the (1 × 2) structures proposed by Pang et al.[39] and by Onishi et al.[40] are both accepted models: based on crystal preparation procedures, the description of the (1 × 2) structure by either one of the "added row" models may be appropriate.

The (1 × 2) reconstructed surface does display differing behavior in the presence of UV light when compared to the (1 × 1) surface, which is unaffected by UV irradiance.[42] When exposed to high photon fluxes of UV light, extensive line defect formation was shown to occur on the (1 × 2) surface. No effect was seen under the same conditions for the (1 × 1) surface. This effect is also mentioned in section 6.3.1.

3. Excitation of Charge Carriers (TiO_2)

The excitation of charge carriers (electron-hole pairs) for TiO_2 materials occurs when the substrate material is exposed to photons of energy higher than the band gap for TiO_2. The sections below address possible mechanisms for lowering the threshold energy for substrate excitation, a topic that has received considerable research interest. Second, this section presents an overview of strategies that have been developed for monitoring the presence of excited charge carriers using either infrared (IR) spectroscopy or electron paramagnetic resonance (EPR) spectroscopy.

3.1. Lowering the Threshold Energy for Excitation

Due to the inherent relatively large band gap characteristic of TiO_2 materials, a great deal of research has focused on lowering the threshold energy for excitation in order to utilize a larger fraction of visible light for conversion to photochemical energy. With its band gap near 3.1 eV, undoped TiO_2 has a photothreshold that extends from the ultraviolet region into the solar spectrum to about 400 nm. This active region of the solar spectrum comprises <10% of its total. By doping TiO_2 with impurities, this threshold energy for photoactivation can be reduced, potentially increasing photoactivity under solar irradiation.

There has been a great deal of interest recently on the use of both nonmetal and transition metal doping, as will be addressed below.

3.1.1. Nitrogen Doping

The idea of doping titanium dioxide materials with nitrogen and other anionic species was first presented by Asahi et al. in 2001.[43] They reported theoretical results from the substitution of C, N, F, P, or S for oxygen atoms in the titania lattice. Results of density of states (DOS) calculations for anatase TiO_2 suggest that substitutional type doping (interstitial type doping and a mixture of both substitutional and interstitial type were both found to be ineffective) using nitrogen is effective due to the mixing of nitrogen 2p states with oxygen 2p states, thus causing a significant decrease in the width of the overall band gap. Similar calculated results were also obtained for S doping; however, S doping is not commonly employed due to its large ionic radius. Asahi et al. further investigated experimentally the use of nitrogen as a substitutional dopant through characterization of $TiO_{2-x}N_x$ films. The doped material, made by sputtering TiO_2 films with N_2/Ar mixtures,[43] was found to consist of both anatase and rutile grain structures and was shown to absorb light

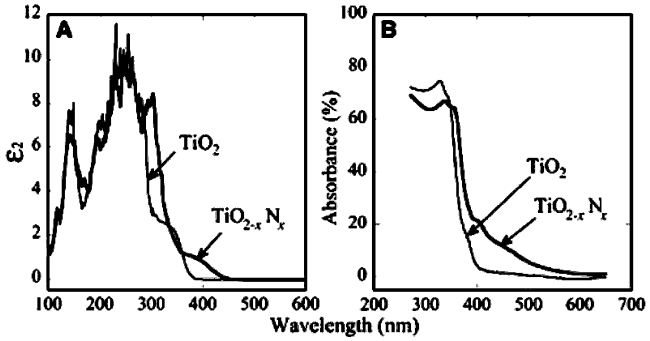

Figure 9. Optical properties of TiO_2 and nitrogen-doped TiO_2: (A) calculated imaginary parts of the dielectric constant; (B) measured optical absorption. Reprinted with permission from *Science* (http://www.aaas.org), ref 43. Copyright 2001 American Association for the Advancement of Science.

below 500 nm. These results are illustrated in Figure 9, where calculated optical properties of a nitrogen-doped TiO_2 film and experimental spectra are compared. It may be seen that light absorption at wavelengths above ~400 nm is characteristic of the nitrogen-doped material.[43]

The photocatalytic activity of the films was analyzed by measuring the decomposition rates for the photo-oxidation of methylene blue as a function of photon energy in addition to the measurement of the photodecomposition of gaseous acetaldehyde.[43] All of the films showed enhanced photocatalytic activity in the visible light region. The films exhibit N 1s XPS features at 396, 400, and 402 eV binding energies. The authors of this work claim that the nitrogen species responsible for the overall band gap narrowing effect exhibits the 396 eV N 1s binding energy. Similar doped powders that did not show the 396 eV XPS feature also did not show enhanced photocatalytic activity.[43]

Recently, a study was published that more clearly investigated the origin of the band gap narrowing by nitrogen doping. In that work,[44] doping of the TiO_2(110) crystal was done in a high-temperature flow reactor, where the crystal could be simultaneously heated and exposed to NH_3 gas at high temperature.[44] After treatment, the crystal was subjected to XPS analysis, where a pair of N(1s) features were revealed, one at 396.5 eV (seen previously and assigned to substitutionally bound N^-) and one at 399.6 eV, which has been attributed to an N···H complex interstitially bound in the TiO_2 lattice.[44] The two-feature XPS spectrum observed for the NH_3-treated samples is comparable to that presented by Asahi et al.[43] However, in Asahi's work, the authors claim that the N 1s XPS feature at 396.5 eV (attributed to substitutionally bound N^-) is related to the photothreshold energy decrease observed, whereas the work in ref 44 finds that the 399.6 eV N(1s) state due to N···H species is the active dopant. A comparison of the XPS spectra from the doped material presented by Asahi[43] and of the NH_3-doped material presented by Diwald et al.[44] is shown in Figure 10. Recently the Diebold group has employed STM and XPS methods to investigate N doping in both rutile(110) and anatase(101) oriented single crystals. N doping induces localized N 2p states within the band gap, just above the top of the valence band, facilitating the production of oxygen vacancies and Ti 3d states within the band gap at elevated temperatures.[45]

A novel test, developed by Fleischauer et al.[46] and others,[47,48] was employed by Diwald et al.[44] to determine the photoactivity of the N···H-doped crystal as a function

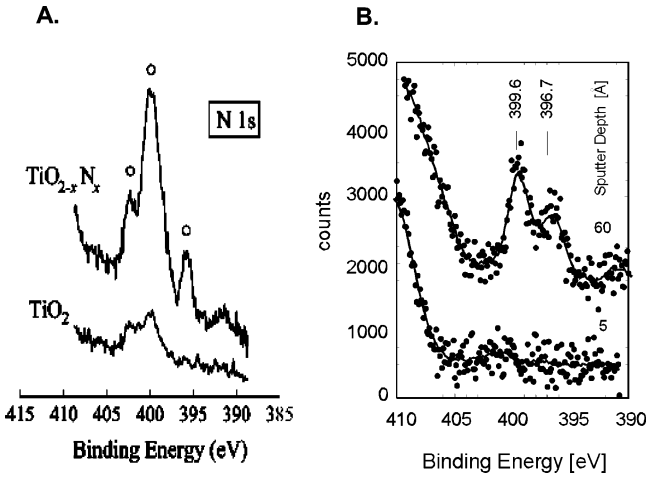

Figure 10. Comparison of the N (1s) XPS data presented (A) by Asahi et al.[43] and (B) by Diwald et al.[44] Panel A is reprinted with permission from *Science* (http://www.aaas.org), ref 43. Copyright 2001 American Association for the Advancement of Science. Panel B is reprinted with permission from ref 44. Copyright 2004 American Chemical Society.

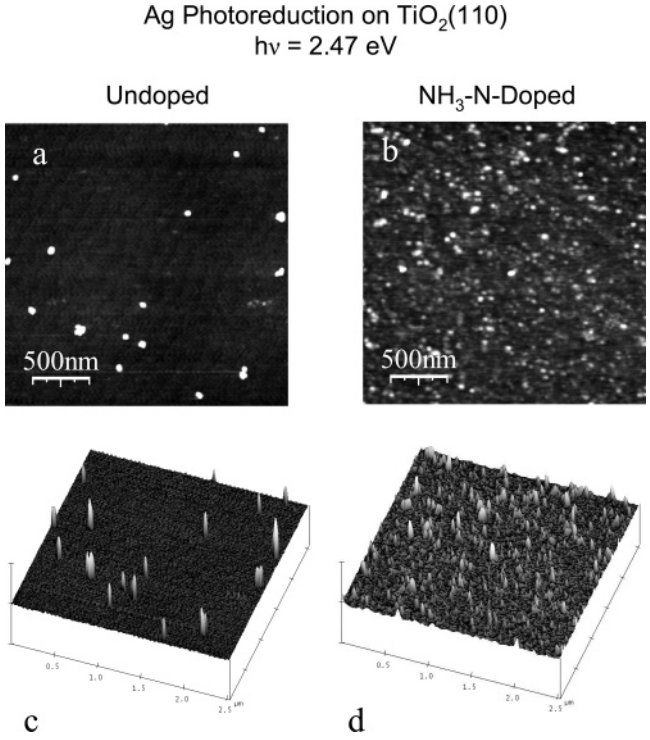

Figure 11. AFM images of Ag clusters deposited on (a) undoped and (b) NH_3-doped TiO_2 rutile single crystals after exposure to UV light. Reprinted with permission from ref 44. Copyright 2004 American Chemical Society.

of photon energy. The results yielded a significant decrease of ~0.6 eV in the photothreshold energy needed for substrate excitation. This test involved the photoreduction of Ag^+(aq) ions to form Ag^0 deposits on the TiO_2 crystal surface. The surface, once exposed to UV, was then imaged using atomic force microscopy (AFM), which was used to evaluate the density and size of Ag^0 clusters produced photolytically. A representative comparison of the AFM images of the NH_3-doped and undoped crystals exposed to UV radiation at 2.47 eV is shown in Figure 11. It should be noted that this effect of N···H doping has been studied for a photoreduction reaction, not for a photo-oxidation reaction. A summary of the results of these studies is shown in Figure 12, where it

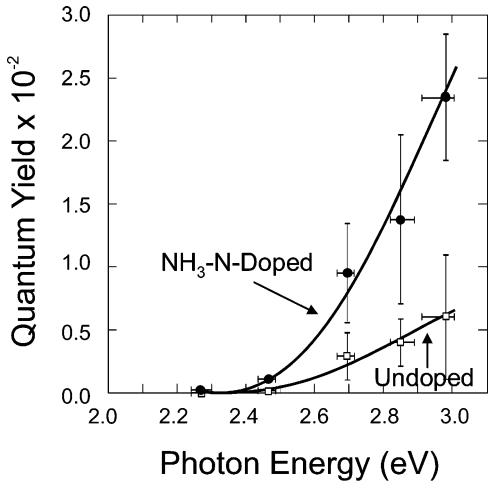

Figure 12. Comparison of the photoactivation of undoped versus NH_3-doped TiO_2(110) single crystals. The points shown were measured using the photoreduction of Ag as measured by AFM and reported in ref 44. Reprinted with permission from ref 44. Copyright 2004 American Chemical Society.

may be seen that an ~0.6 eV decrease in the photothreshold is seen for the N···H-doped TiO_2 crystal compared to undoped TiO_2.

Prior to the work done where NH_3 was used as a dopant,[44] doping of TiO_2(110) was also attempted by Diwald et al.[49] using a high-energy ion gun (in UHV) to implant the TiO_2(110) using a N_2/Ar^+ mixture.[49] After 3.0 keV of N_2^+ implantation, the crystal was annealed extensively, allowing diffusion of implanted N atoms further into the bulk of the crystal. The crystal photoactivity was then tested using the photodesorption of adsorbed O_2 at various photon energies. XPS, TEM, and SIMS were also used to examine the nature and depth of the implanted nitrogen species. Results of this work showed an *increase* in the photothreshold energy, opposite to that observed by others. The XPS data for the ion-implanted surface show a single 396.5 eV N(1s) feature attributed to substitutional nitrogen, assigned as N^-, therefore suggesting that substitutionally bound N^- alone is not responsible for the decrease in the photothreshold of TiO_2(110) as suggested by Asahi et al.[43] Work done by Burda et al.[50] on nitrogen-doped TiO_2 nanoparticles reports substitutionally bound nitrogen as the active dopant species, in agreement with Asahi.[43] This work, however, differs from that of Asahi in that the measured N 1s XPS feature exhibits a binding energy near 400 eV, and no peak is measured at or near 396 eV as found by Asahi.[43] Other authors also report N 1s XPS features for nitrogen-doped titania at 400 eV,[51] yet assignment of this species remains an issue. Burda et al. reports that the substitutional type nitrogen species responsible for the observed increase in the measured photocatalytic activity in the visible region is due to N−O type bonding as reported in ref 52. Thus, although Diwald et al.[44] and Burda et al.[50] agree that a nitrogen species with an N 1s binding energy near 400 eV is an active dopant, their assignments of its chemical nature differ.

Hoffmann et al.[53] have also extensively investigated the effect of nitrogen doping on titania materials. That work focused on investigating the photo-oxidation of organics over N-doped materials prepared using a method earlier reported by Burda and Gole.[54] Hoffmann et al.[53] report results suggesting that organic molecules such as methylene blue, commonly employed by others to monitor photo-oxidative processes, may be uninformative as to the actual activity of

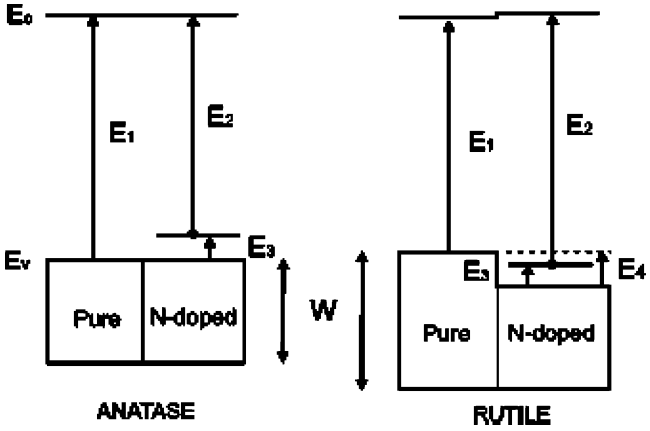

Figure 13. Comparison of the calculated electronic structures for N-doped anatase and rutile TiO_2 as described by Selloni et al.[55] Reprinted with permission from ref 55. Copyright 2004 American Physical Society.

the TiO_2. It is likely that photo-oxidation of methylene blue and other dyes occurs through direct excitation and degradation by UV or visible illumination. These dyes are oxidized with or without the presence of TiO_2[53] and may give false results when used to investigate photo-oxidation chemistry on TiO_2.

Density functional theory calculations have addressed the variances in the photoactivity measurements[55] considering both anatase and rutile type samples that have been substitutionally doped with nitrogen. The conclusions of this work are profound. For anatase samples, substitutional N doping results in a decrease in the photon energy necessary to excite the material; for rutile TiO_2 materials, the opposite effect is observed and is attributed to the contraction of the valence band and the stabilization of the N 2p state, thus causing an overall increase in the effective band gap in agreement with the work of Diwald et al.[49] For anatase TiO_2, substitutionally bound nitrogen atoms create localized occupied electronic states (N 2p in character) above the top of the O 2p valence band. The creation of this occupied electronic state has also been shown experimentally.[56,57] As a result, the mechanism for photoexcitation of N-doped anatase is most probably direct excitation of electrons from the N 2p state located within the band gap of the TiO_2, into the conduction band. The measured inter-band-gap density of states has been postulated to reduce the rate of electron−hole pair generation, which may readily occur without the presence of these states.[56] A schematic diagram explaining this effect for anatase and rutile is shown in Figure 13, where for rutile TiO_2 the suppression of the top of the valence band is observed for N doping. Similar calculations recently presented by other authors[58] agree with the work presented by Selloni et al.[55]

The difference in the dopant states for substitutional versus interstitial type impurities in anatase TiO_2 was investigated both experimentally on TiO_2 powders using electron paramagnetic resonance spectroscopy (EPR) and XPS and theoretically using DFT calculations.[59] This work[59] reveals a distinct N 1s XPS feature at 400 eV, but the authors note that preparation methods and differing experimental conditions can drastically affect the nature of the measured XPS signals. In addition, the authors also point out the probability that the observed XPS feature ascribed to N 1s transitions may originate from the presence of any number of differing nitrogen species. Although the EPR characterization of the nitrogen species in the anatase material considered in this work is inconclusive, the theoretical findings show very distinct differences in the calculated electronic structure for substitutional versus interstitial type nitrogen. Both types of impurities are found to add localized states within the band gap. For substitutional type nitrogen, these states are located 0.14 eV above the valence band, and for interstitial type nitrogen species (referred to as N−O), the localized states are calculated to lie 0.73 eV above the valence band. In addition, these calculations have also found that there is a large decrease in the formation energy for oxygen vacancies as a result of additional nitrogen atoms in the lattice. Therefore, oxygen vacancies are most probably induced by N doping of TiO_2. This work, although quite useful in realizing the actual electronic nature of doped titania materials, does not address the actual observed change in the photocatalytic activity as a result of impurity addition.

In summary, there is a great deal of literature existing on the topic of nitrogen doping of TiO_2 materials, most of which agrees that the addition of nitrogen to the lattice of TiO_2 results in increased photocatalytic activity at lower photon energies. Theoretical results have also clearly illustrated that

Table 1.

author (ref)	method/substrate	dopant type	result
Asahi et al.[43]	theoretical: density of states calculations experimental: sputtering of rutile/anatase TiO_2 films with N_2/Ar	substitutional; mixed (substitutional and interstitial); interstitial	substitutional type dopant causes increase in photocatalytic activity; authors correlate finding to N ls binding energy at 396 eV; interstitial or mixed dopant states are found to be ineffective
Hoffmann et al.[53]	experimental: NH_3-doped anatase TiO_2	not characterized	doped TiO_2 material absorbs light up to 520 nm, but fails to completely photo-oxidize $HCOO^-$
Burda et al.[50]	experimental: chemical doping method for TiO_2 nanoparticles	substitutional	substitutional type dopant measured at 400 eV due to N−O type bonds in the lattice
Diwald et al.[44,49]	experimental: high-temperature gaseous doping with NH_3 [also TiO_2(110)] sputtering of rutile TiO_2(110)	interstitial (high-temperature treatment) substitutional (sputtering treatment)	interstitial dopant (400 eV N 1s binding energy) is active dopant, suppressing photothreshold; substitutional dopant (396 eV N 1s binding energy) increases photothreshold energy
Di Valentin et al.[55]	theoretical: anatase and rutile TiO_2	substitutional	substitutional dopant causes decrease in photothreshold energy for anatase samples only; for rutile, an increase in the photothreshold energy is observed
Di Valentin[59]	theoretical and experimental: anatase	substitutional and interstitial	both dopant types create a discrete energy level within the band gap, suggesting that either dopant may cause a decrease in the photothreshold energy for TiO_2 activation

the addition of either substitutionally or interstitially bound nitrogen species results in localized N 2p states that are discrete levels above the valence band, in contrast to past reports which suggested valence band broadening. Table 1 presents a compilation of the literature dealing with nitrogen doping on TiO_2.

3.1.2. Carbon Doping

In addition to investigations of TiO_2 doping with nitrogen as discussed above, carbon has recently received considerable interest as a nonmetallic dopant in TiO_2 materials. Carbon was first investigated as a substitutional type dopant in TiO_2 by Khan et al.,[60] who studied the band-gap energy through measurement of the efficiency of water splitting similar to the method first used by Honda and Fujishima.[61] The material studied in this work was chemically modified TiO_2 synthesized using flame pyrolysis of a Ti metal sample, an ill-defined material compared to single-crystalline TiO_2. Carbon was incorporated during the pyrolysis process that was carried out in the presence of combustion products (CO_2 and H_2O).[60] The resulting TiO_2 film was characterized by X-ray diffraction (XRD) and found to be mainly rutile. Measurements of the photocurrent at various applied voltages show increased activity for the carbon-doped films when compared to undoped materials that were fabricated using the same method. A significantly reduced band gap of 2.32 eV is reported for the carbon-doped material, compared to 3.0 eV for undoped rutile. The proposed mechanism for this action is band-gap narrowing.[60]

Since the initial experimental investigation of carbon-doped TiO_2, other authors have investigated carbon doping in TiO_2 both experimentally[62−64] and theoretically.[58,65] Sakthivel and Kisch have shown that carbon incorporation into TiO_2 powders causes a 4−5-fold increase in activity for the degradation of 4-chlorophenol by UV light compared to nitrogen-doped TiO_2 materials. The preparation method for the samples presented in ref 62, although similar to that presented by Khan et al.,[60] results in carbon-containing species, either elemental adventitious carbon or carbonate species. This finding is in contrast to that presented by Khan,[60] who report the presence of substitutionally bound carbon. Tachikawa et al.[63] investigated carbonate-species-doped TiO_2 (anatase) and found that although UV-induced charge carriers are generated more readily for carbonate-doped TiO_2, no evidence for enhanced photo-oxidation chemistry is measured. The authors attribute this finding to a possible decrease in the mobility of the photogenerated holes, which participate in the photo-oxidation step. This may be directly related to significant trapping of charge carriers that occurs upon photoexcitation and is directly dependent on the incoming photon flux and the density of impurity sites (which may act as trapping sites) in the surface or the bulk of the material.[66]

The action of carbon type dopants in both anatase and rutile forms of TiO_2 has been addressed theoretically.[65] The authors investigated the effect of both substitutional and interstitial type carbon dopants in the anatase and rutile forms of TiO_2. The stability of the dopant species as a function of oxygen partial pressure was investigated. In addition, the electronic structure of each material after the addition of either substitutional or interstitial type dopants was calculated. For both rutile and anatase TiO_2, it is found that the same general trends are realized for both substitutional and interstitial types of carbon dopants as a function of the oxygen partial pressure. At low partial pressures of oxygen, substitutional type doping of carbon atoms substituting for oxygen atoms is favored. In addition, the formation energy for oxygen vacancies decreases with the presence of the carbon dopant. At high partial pressures of oxygen, both interstitial and substitutional (where carbon binds to titanium atoms) carbon dopants are present. For both anatase and rutile, the presence of both types of carbon dopants causes the formation of localized occupied band gap states that vary in energy on the basis of the dopant type, the presence or absence of oxygen vacancies, and the background partial pressure of oxygen. The presence of these states gives rise to the decreased energy necessary for excitation of either material, as reported experimentally. Figure 14 shows the various site locations considered for C atom doping in TiO_2. Figure 14a shows the substitution of a C atom for an O atom (C_{S-O} site). In Figure 14b is shown C atom substitution at a Ti site (C_{S-Ti} site). Figure 14c shows C atom insertion in an interstitial site (C_I site). In Figure 14d is shown C atom insertion near an O vacancy ($C_I + V_o$ site). The yellow spheres represent O atoms, the small brown spheres Ti atoms, and the black spheres C atoms.[65]

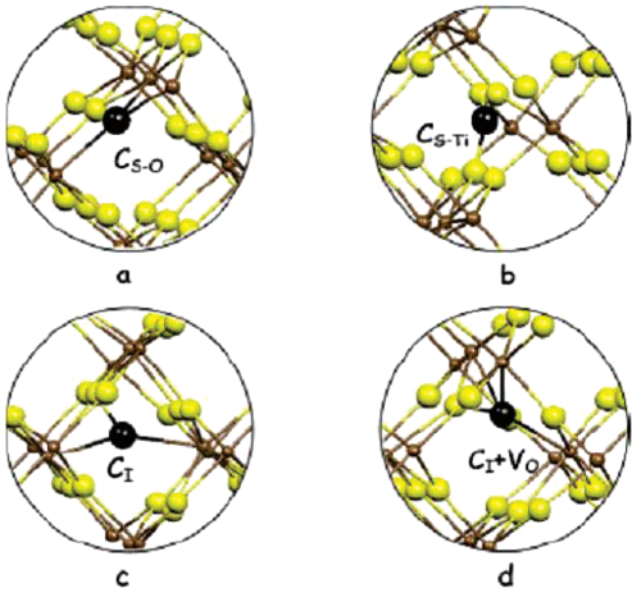

Figure 14. Partial geometry for various models for the doping of carbon into TiO_2. See text for an explanation of the figures. Reprinted with permission from ref 65. Copyright 2005 American Chemical Society.

3.1.3. Transition Metal Dopants

Doping with transition metal ions including Cr,[67] V,[68] Fe,[69,70] Pb,[71] Cu,[72] and others has been investigated. Doping with these metal ions has shown both positive and negative effects on the photocatalytic activity of TiO_2; a number of authors claim that although metal ion doping should decrease the photothreshold energy of TiO_2, the metal ion may also serve as a recombination center for electrons and holes, thus diminishing the overall activity of the photocatalyst.[73] Karvinen et al.[74] have theoretically investigated the role of transition metal dopants in both anatase and rutile TiO_2 models. For anatase TiO_2, the addition of Ti^{3+}, V^{3+}, Cr^{3+}, Mn^{3+}, and Fe^{3+} caused significant band gap narrowing; however, for the rutile system, no effect was found.[74] Hoffmann et al.[73,75] have investigated a great number of metal ion dopants in TiO_2 powders with the specific aim to measure

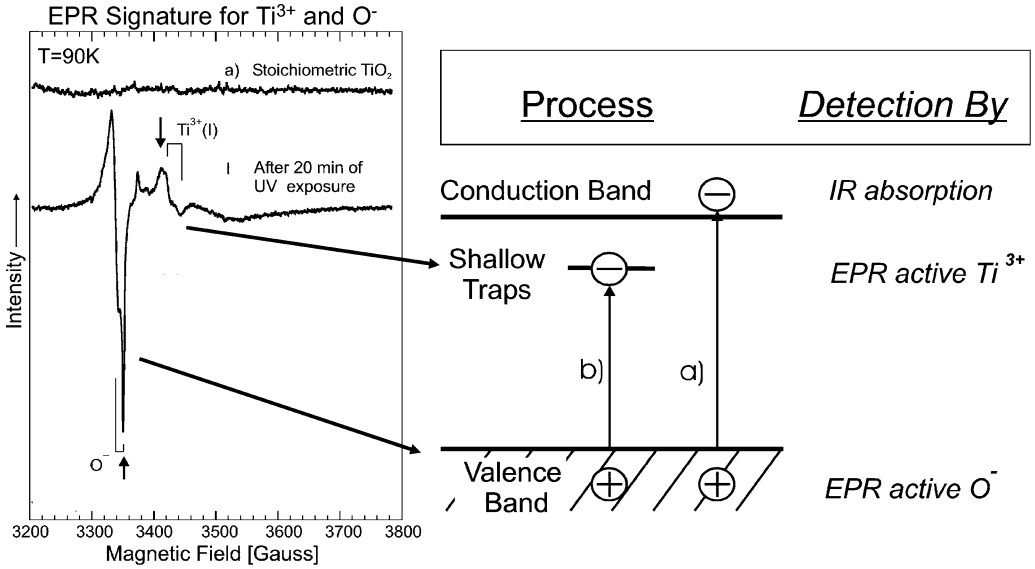

Figure 15. Characteristic EPR signature for photogenerated electrons and holes in fully oxidized anatase TiO_2. The right-hand schematic shows the location of the conduction band electrons (detected by IR spectroscopy), electrons trapped at shallow trap sites (EPR detection), and charge carrier holes present in the valence band (EPR detection). Reprinted with permission from ref 27. Copyright 2005 American Chemical Society.

the photoactivities of the resulting material. A mixture of both positive and negative effects was reported. Choi et al.[73] have carried out an exhaustive study of the effects of ion doping of quantum-sized TiO_2 nanoparticles in the 2−4 nm size range, using coprecipitation of the dopant ion and the TiO_2 from a solution of titanium tetraisopropoxide solution undergoing controlled hydrolysis. Doping with Fe^{3+}, Mo^{5+}, Ru^{3+}, Os^{3+}, Re^{5+}, V^{4+}, and Rh^{3+} was carried out to 0.1−0.5 atomic percent, and the photoreactivity toward chlorinated organic molecules was increased for both oxidation and reduction reactions. The quantum yields obtained during photolysis with steady light intensity were quantitatively correlated with the measured transient charge carrier absorption signals. They report that the photoreactivity of the doped TiO_2 increases as the dopant concentration is increased but that there exists a complex dependence on dopant concentration, dopant energy state in the lattice, the d-electron configuration, the distribution of dopants, the electron donor concentration, and the light intensity.

Much additional work has been done on metal doping of TiO_2, but a detailed understanding from a surface science viewpont has not yet been achieved.

3.2. Monitoring Charge Carrier Excitation and Recombination

Berger et al.[27] reported the detection of mobile charge carriers in TiO_2 powders by either electron paramagnetic resonance spectroscopy or infrared spectroscopy. These tools complement each other quite well for studies of this nature. In this work, it was shown that under continuous UV illumination, photogenerated electrons are either trapped at localized states within the band gap (Ti^{3+} centers), where they are measured by EPR spectroscopy, or promoted to the conduction band, where they are unable to be detected by EPR but are able to be easily measured by IR spectroscopy. Photoexcited hole species are able to be detected also using EPR and are measured as O^- species, which originate from lattice O^{2-} ions. Using these methods, the lifetime of the photoexcited electrons and holes can be measured and is found to be on the order of hours at low temperature ($T =$ 90 K). At room temperature, the recombination process is much faster, and the photogenerated electrons and holes recombine rapidly. Figure 15 illustrates the detection of photogenerated electrons and holes via either EPR or IR spectroscopy.

3.2.1. IR Spectroscopy as a Tool for Monitoring Conduction Band Electrons

The energetic promotion of electrons from the valence band to the conduction band in semiconductors can occur in a number of ways. As discussed earlier, promotion of electrons via UV irradiation with photons greater than the band gap energy leaves electrons in states near the conduction band where, at low temperature, they may be stored for long periods of time. For a powdered mixed oxide material (TiO_2-SiO_2), Payanotov et al.[76] have observed the presence of conduction band electrons produced upon thermal annealing in a vacuum. The same is observed for pure TiO_2, unmixed with SiO_2.[77] This effect is directly related to the thermally activated production of defects within the material as the time and/or temperature of the annealing process increases. The shallow-trap defect site (probably Ti^{3+}) then provides electrons to the conduction band by thermal excitation from the defect state at the temperature of the measurement (476 K), as shown schematically in Figure 16.

This process is sometimes referred to as "metallization" of the semiconductor. Free carriers (electrons) promoted to the conduction band behave approximately as delocalized electrons in an infinite-walled three-dimensional box. The high density of states provides a continuum of electronic excitations, resulting in an increase in the featureless background of the infrared spectrum as excitations over a wide energy range in the infrared region combine to produce the broadband background absorption. This phenomenon is called Drude absorption, as found in metals.[78] In semiconductors, detection of excitation to delocalized conduction band electron states is done by infrared absorption spectroscopy, and a broad structureless absorption increase is measured, as shown in Figure 17. The description of these delocalized electrons, their coupling to phonons, and the

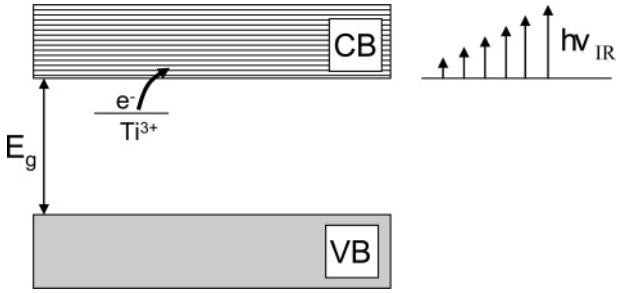

Figure 16. Schematic diagram depicting the thermally activated charge injection of electrons from shallow trap sites into a continuum of states in the conduction band of this wide-band gap semiconductor. IR excitation in the CB is also indicated.

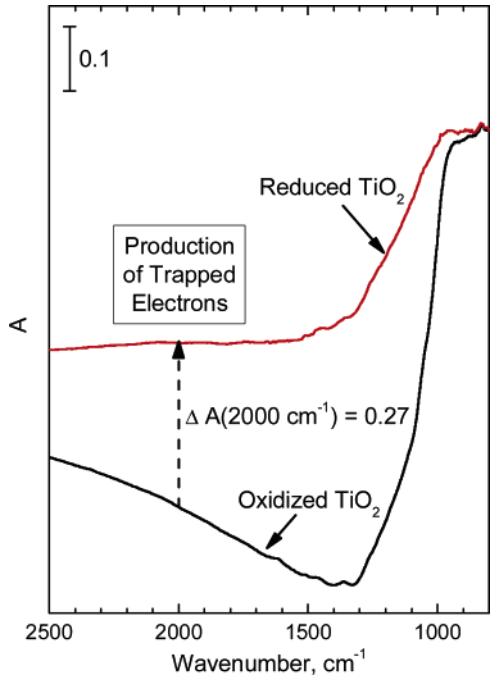

Figure 17. IR absorbance spectra for oxidized and reduced TiO_2. Trapped electrons are measured by the increase in the background absorbance measured at 2000 cm^{-1}. Reprinted with permission from ref 27. Copyright 2005 American Chemical Society.

formation of polarons as a result of lattice distortion are topics beyond the scope of this review. Hoffmann and coworkers[79,80] have detected transient and persistent diffuse reflectance infrared signals due to the population of conduction band electrons upon irradiation of TiO_2 powders with supra band gap light, where the baseline IR absorption for TiO_2 rises immediately upon UV irradiation.[27,80] In addition, the observed response partially recovers in the dark and fully recovers upon the addition of oxygen.

The decay of the electron concentration in the conduction band, produced by UV excitation, is shown in Figure 18. Here the broad background spectrum is observed in reflectance spectra to decay over periods greater than hundreds of minutes at 300 K. Spectrum a was produced by UV irradiation and was measured 13 min after UV excitation was discontinued. Over time periods extending to 135 min after irradiation, spectra b−d were measured. The final spectrum, Figure 18e, corresponds to full relaxation of the excited system. The inset shows a plot of $\log(S(\lambda/\mu))$ versus $\log(\lambda/\mu\text{m})$, which is linear for all spectra a−d, indicating that $S(\lambda) = A(\lambda^p)$ for all stages of relaxation. The value of the exponential $p = 1.73$, indicative of a constant spectral shape

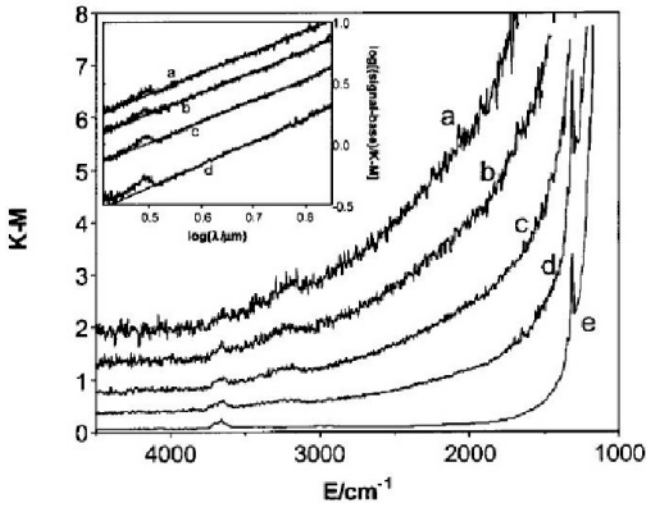

Figure 18. Diffuse reflectance infrared Fourier transform spectra of powdered TiO_2 following UV irradiation. Spectra a−e correspond to various relaxation times ranging up to hundreds of minutes at 300 K. (Inset) The line shape of the broad background remains constant as the decay of electrons in the conduction band occurs. Reprinted with permission from ref 80. Copyright 2002 American Chemical Society.

independent of the degree of relaxation, shows that a single state containing trapped electrons is responsible for the observed background shift throughout the IR region. A value of $p = 1.5$ is expected for electron momentum conservation with acoustic phonons in a semiconductor according to ref 80. An infrared band near 3390 cm^{-1} is assigned to an electronic excitation and does not shift with D substitution for H in surface hydroxyl groups.[80]

Detection of photoproduced conduction band electrons by IR spectroscopy was also earlier reported by Yamakata et al.,[81] who measured the excitation of powdered Pt/TiO_2 materials activated by short time scale laser pulses. Here, as in work presented by Berger et al.,[27] the transient IR absorbance over a wide range of wavenumbers (3000−900 cm^{-1}) is monitored before, during, and after the photoexcitation step. Yamakata et al.[81] observed a peak in the IR absorbance at time = 0 (onset of 10 ns laser pulse) and measure decay kinetics for the concentration of conduction band electrons as measured by the IR background absorbance. The decay kinetics are highly fractal, which means that fits may only be made using a wide range of rate constants. This is illustrated in Figure 19, where four time domains of the decay are presented ranging from microseconds to seconds. Fits were done using six decay constants.

The reported decay kinetics for photogenerated electrons after excitation is shown to be first-order, which is in contrast to results presented by these authors for work done on $TiO_2(110)$ at 110 K, where second-order recombination kinetics are inferred (see section 4.2 and ref 66). The explanation presented by Yamakata et al. for first-order decay kinetics is the following: in colloidal TiO_2 particles, where only low concentrations of electron−hole pairs accumulate, the kinetic rate law is first-order in nature, whereas when higher concentrations of electron−hole pairs are present, the kinetic rate law is second-order in nature.[82] This topic is further addressed in section 4.2.

Early work done on the detection of trapped electrons in the conduction band as measured by IR spectroscopy was reported by Baraton et al.[83] The authors reported the use of TiO_2 powders as a sensor material for oxidizing or reducing

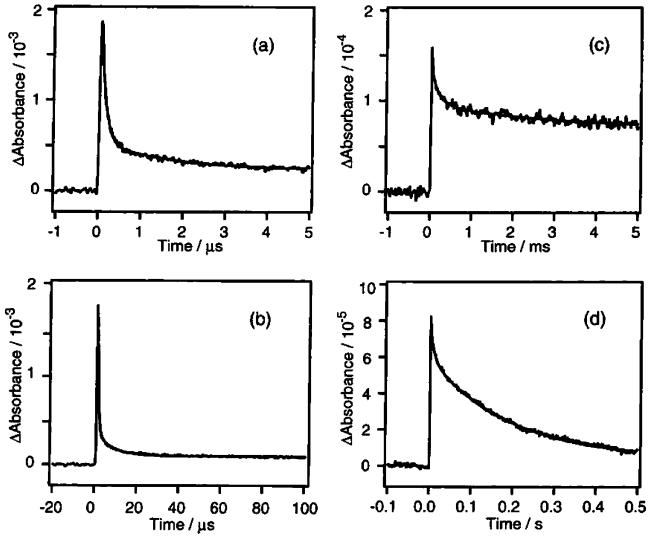

Figure 19. Decay curves of the IR absorption at 2000 cm^{-1} for Pt/TiO_2 powder following laser pulse excitation at 355 nm with an energy of 7 mJ. Reprinted with permission from ref 81. Copyright 2001 Elsevier B.V.

agents. In the presence of an oxidizing agent, electrons are removed from the conduction band by the adsorbate, thus decreasing the background IR absorbance. The opposite effect was measured for reducing agents that inject electrons into the conduction band, thus increasing the background IR absorbance.[83] This work demonstrates the use of metal oxide materials for gas sensors using IR spectroscopy as a detection tool.

3.2.2. Electron Paramagnetic Resonance Spectroscopy (EPR)

EPR is widely employed for the detection of photoexcited charge carriers in metal oxide materials. Early work on the use of EPR for the study of UV-induced effects on TiO_2 powders has been studied extensively and reported in review format.[84,85] Work done by Howe and Grätzel[86] reports on the trapping of photogenerated electrons and holes in the bulk and surface region of hydrated anatase TiO_2 polycrystalline material at very low temperatures (4.2 K). Electrons are trapped at low temperatures at localized Ti^{4+} sites (to produce Ti^{3+}) within the bulk of the material, and holes are trapped as lattice oxide ions (O^-) below the surface. As mentioned above and reported by Berger et al.[27] the photogenerated electrons and holes exhibit a lifetime of hours at 90 K. A direct linear correlation between the concentration of photogenerated electrons (Ti^{3+} species) and holes (O^- species) measured by EPR spectroscopy on polycrystalline anatase TiO_2 exists and is depicted in Figure 20. The deviation from linearity suggests that at high UV light intensities a fraction of photogenerated electrons are transferred to the EPR-silent conduction band (due to the finite concentration of Ti^{3+} electron-trap defect sites), where they can be measured using IR spectroscopy as discussed in section 3.2.1.

For reduced samples, where oxygen vacancies are created in the bulk of the material, the EPR signal is identical to that of trapped (Ti^{3+}) photogenerated electrons that are created in the presence of UV irradiation: Ti^{3+} signals are clearly measured in each case. However, for reduced TiO_2, the EPR signal intensity is enhanced by a factor of 25, suggesting a greater concentration of thermally produced

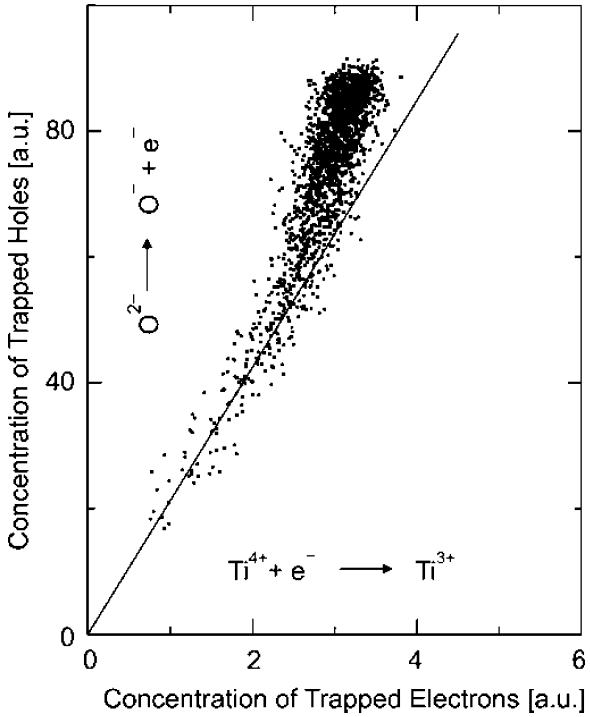

Figure 20. Correlation between the concentration of trapped electrons and trapped holes as observed by EPR spectroscopy of photoexcited TiO_2. At high UV light intensity, trapped electrons are excited into the conduction band (EPR silent). As a result, the concentration of trapped electrons becomes unequal to the concentration of trapped holes and a break in the linear correlation occurs. Reprinted with permission from ref 27. Copyright 2005 American Chemical Society.

electrons after annealing the TiO_2 to 950 K when compared to the concentration of photogenerated trapped electrons observed for oxidized TiO_2. Little to no signal is observed for O^- holes in thermally reduced TiO_2. When the reduced material is further exposed to sub-band-gap UV irradiation, a photobleaching effect occurs, where all of the characteristic electron and hole EPR signatures are eliminated. This effect can be explained by the ionization of trapped electrons located in inter-band-gap states.[27]

4. Recombination of Excited Electrons and Holes

4.1. Shockley–Read–Hall Recombination at Trap Sites

The concentration of charge carriers upon UV excitation in any semiconductor is reduced by the inherent recombination process that may occur, leading to the destruction of active electron−hole pairs. For TiO_2, this action can be explained by the Shockley−Read−Hall model for nonradiative recombination, which describes the capture of mobile electrons and/or holes at trap sites within the semiconductor.[87,88] Once trapped, the electron (or hole) is then annihilated via recombination with holes from the valence band (or electrons from the conduction band). The active sites for electron or hole trapping may vary and are usually described as defect states within the crystal due to interstitial atoms, defect states, or grain boundaries and the like. In the Shockley−Read−Hall mechanism, as schematically depicted in Figure 21, four transition processes may occur: (1) electron capture; (2) electron emission; (3) hole capture; or (4) hole emission. This model assumes that the

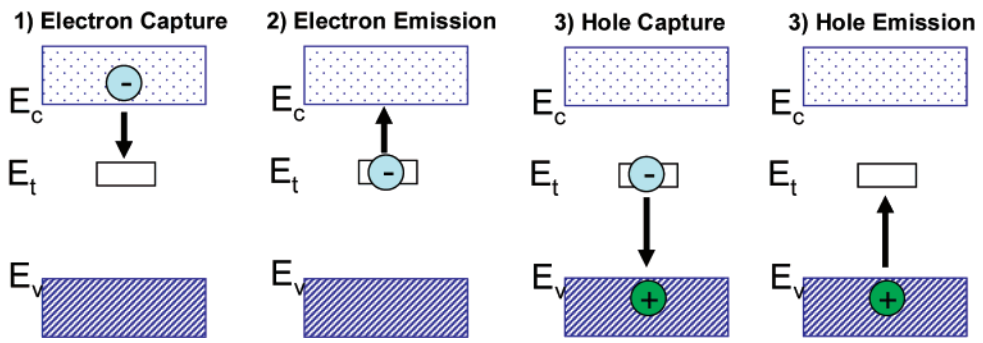

Figure 21. Schematic diagram showing the four electronic transition processes that may occur for the charge carrier recombination as described by ref 88. Reprinted with permission from ref 88. Copyright 1952 American Physical Society.

semiconductor is non-degenerate and that the density of trap sites is relatively small compared to the majority carrier density present in the material. For a TiO_2(110) single crystal the concentration of hole-trapping sites was estimated by Thompson et al.[66] to be on the order of 2.5×10^{18} cm^{-3}, which is equivalent to an atomic fraction of 3×10^{-5} of the bulk atomic sites in the crystal.

4.2. Kinetics of Recombination

The kinetic processes by which photochemistry on TiO_2 is governed have been investigated using a simple surface photochemical reaction, namely, the photon-induced desorption of molecular oxygen from TiO_2(110).[66] It is known that oxygen molecules are adsorbed at oxygen-vacancy defect sites[89−91] in the surface and that they become negatively charged as O_2^- species.[92−94] This will be discussed in greater detail in section 5.1. To study the excitation of photogenerated charge carriers, the effect of the incident light intensity on the rate of photodesorption of O_2 was investigated. This work builds on that of other authors who have reported a correlation between reaction rate or photo-oxidation rate to the square root of the incident light intensity.[95−100] Those experiments are less refined than the work presented in ref 66 that involves carefully controlled studies of a simple photoprocess that occurs in ultrahigh vacuum on a planar single crystal of TiO_2 with known surface structure[9] and known surface defect density[20] and in the absence of solvents and surface-bound chromophores. In addition, the photon flux and photon energy are well-known. Thus, quantification of the rate of a well-defined photoprocess compared to the photon flux received by the planar single crystal surface can be accurately made in this model system involving a TiO_2(110) single crystal. A kinetic model was developed and is presented below and in ref 66:

$$h\nu + \mathrm{TiO_2} \xrightarrow{k_1 F_{h\nu}} \mathrm{e^- + h^+} \quad (1)$$

$$h^+ + T \xrightarrow{k_2} \mathrm{T^+}\ \text{(hole capture by a hole trap)} \quad (2)$$

$$\mathrm{e^- + h^+} \xrightarrow{k_3} \text{heat (on recombination sites)} \quad (3)$$

$$\mathrm{h^+ + O_2^-(a)} \xrightarrow{k_4} \mathrm{O_2(g)}\uparrow \quad (4)$$

After hole trap filling by reaction 2 and assuming a fast equilibrium is established between the e−h pair formation (step 1) and the recombination (step 3), the rate of O^-_2(a) photodesorption will be, according to the steady-state approximation

$$-\mathrm{d}[O_2^-(\mathrm{a})]/\mathrm{d}t = k_4[O_2^-(\mathrm{a})]\left[\frac{k_1}{k_3}\right]^{1/2} F_{h\nu}^{1/2} \quad (5)$$

where the recombination process (step 3) is second-order in the hole concentration, [h], leading to a desorption rate containing the factor $F_{h\nu}^{1/2}$. This assumes that at steady state conditions, $[e^-] \approx [h^+] =$ constant. The linear correlation between the yield of photodesorbing oxygen and the square root of the incident light intensity is shown in Figure 22. Further discussion of Figure 22 will follow later.

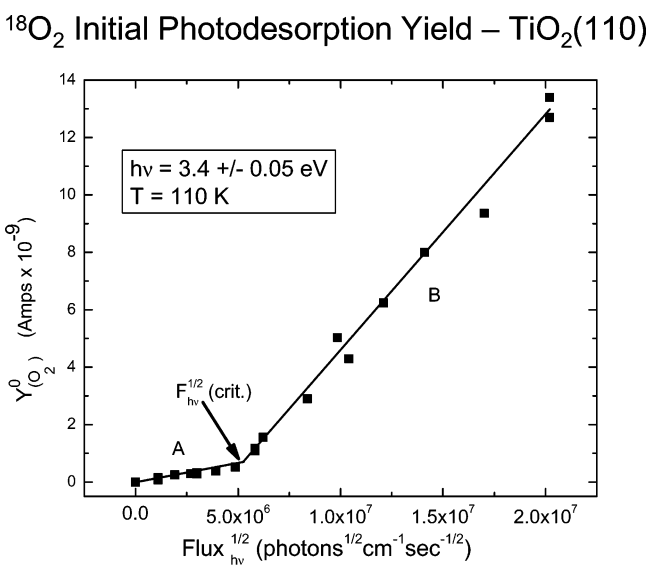

Figure 22. Yield of photodesorbing oxygen for increasing photon flux. A linear correlation between the yield of photodesorbing oxygen and the square root of the photon flux proves that the recombination process is second order. Reprinted with permission from ref 66. Copyright 2005 American Chemical Society.

Much work on photochemical oxidation reactions in solution has been carried out. Here, additional complexities having to do with solvent effects, pH effects, etc., are found, and in some conditions, reactions are studied where diffusion of the reactant to the immersed TiO_2 particle surface is rate determining. Recent work by Cornu et al.[101,102] has shown that the dynamics measured in the fast time regime (picoseconds, and somewhat above) is irrelevant to surface photochemistry and that slower kinetic processes determine the reaction kinetics.[101] For the photo-oxidation of formate

ions in aqueous solution, the rate is found to be proportional to $F_{h\nu}^{0.61}$ for a particular range of light intensity.[101] By using interrupted illumination methods, different photo-oxidation kinetic regimes have been studied. This work has been continued in a later study of the photo-oxidation of methyl orange, where the influence of pH has been studied. It has been found that the chemical intermediates persist longer than a few milliseconds, suggesting that fast laser-driven photoprocesses are not involved in the chemical kinetics of TiO_2-mediated surface photochemical processes.[102]

4.3. Evidence for Trap Filling–Photodesorption of O_2

From eq 5, the instantaneous rate of photodesorption is measured for the initial pulse height of $^{18}O_2$ that desorbs from the TiO_2(110) surface as supra band gap light is exposed to the crystal face. The initial photodesorption pulse is termed the initial yield of photodesorbing oxygen, $Y^0_{O_2}$. Figure 22 shows the dependence of $Y^0_{O_2}$ on the magnitude of $F_{h\nu}^{1/2}$. Two linear branches with differing slopes, A and B, are measured. Branch A corresponds to a photodesorption process of low efficiency, where significant hole trapping results in a lower probability for photogenerated holes to reach the surface. In branch B, the large concentration of photogenerated holes saturates the hole-trapping centers, and in this region of high $F_{h\nu}$, there is an increase in the number of holes that are able to reach the surface. As shown in Figure 23, about each trapping site (T) there is a spatial range in which photogenerated holes produced in this region will, on average, reach the T site and become trapped. Photogenerated holes not trapped at T sites will reach the surface, where the holes can produce O_2 photodesorption with a probability governed by the factors $F_{h\nu}^{1/2}$ and $[k_1/k_3]^{1/2}$ in the series of experiments at constant $[O_2^-(a)]$.

Most studies of the photochemical filling of trap states have concerned electron trapping. When an electron trap becomes filled, the Fermi level crosses the energy level of the trap and the trap becomes inactivated for further electron capture. This trap saturation effect can enhance the lifetime of photogenerated charge carriers and can improve the quantum yield of carriers at higher light intensities.[103] These ideas may also apply to hole trapping in TiO_2, as demonstrated in Figure 22.

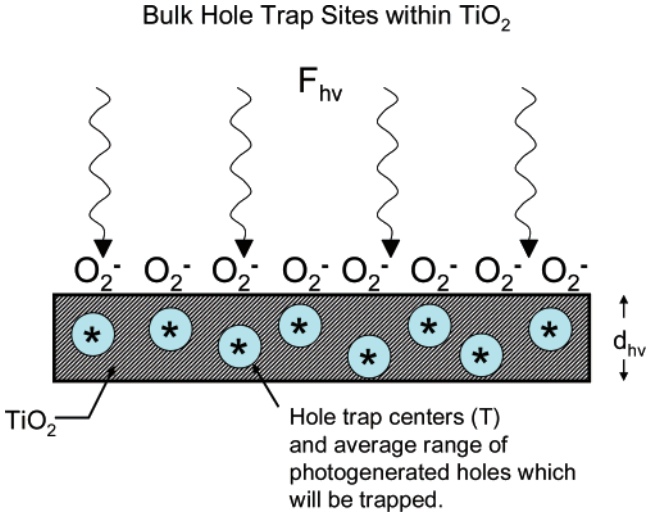

Figure 23. Schematic diagram showing the active range of sites for hole trapping. Reprinted with permission from ref 66. Copyright 2005 American Chemical Society.

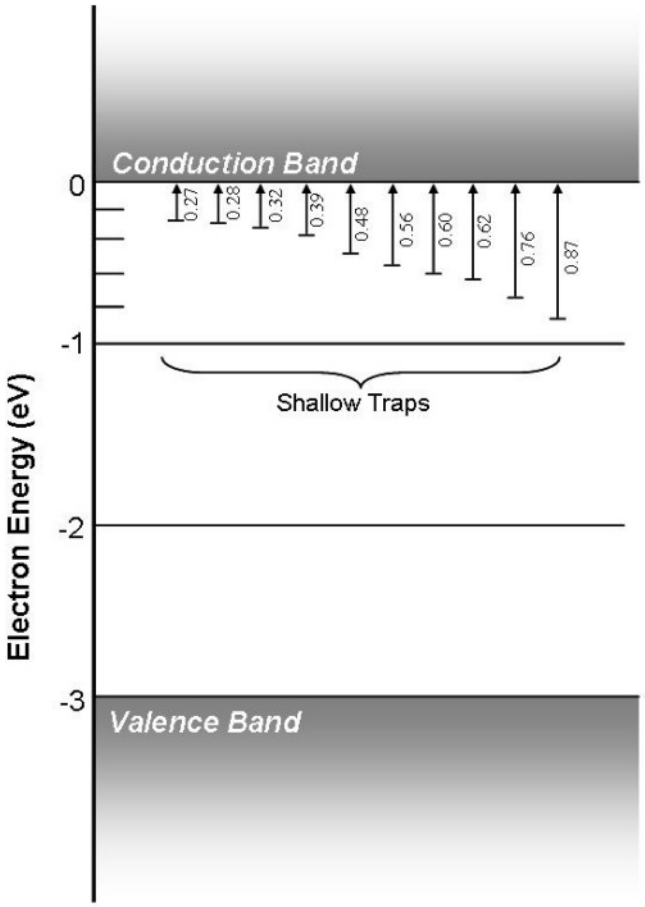

Figure 24. Energy levels measured for Ti^{3+} interstitial species in a TiO_2 rutile single crystal. Adapted from ref 106.

Trap filling has been observed in semiconducting silicon substrates[104,105] and has also been suggested for rutile single crystals,[106] polycrystalline TiO_2 electrodes,[103] and ZnO nanoparticles.[107] The saturation of deep trap levels results in enhanced carrier mobility and carrier lifetime. Schwarzburg[103] finds results similar to those presented in Figure 22; however, the authors investigate charge carrier mobility via transient photocurrent measurements. An inflection point in the measured photocurrent due to the saturation of deep trap levels was reported there.[103] Nelson et al.[108] reports that multiple trapping events may occur at a broad energetic distribution of trap states located within the band gap region. This broad exponential energy distribution of trap states is responsible for the large range of measured recombination times.[108] Ghosh et al. also report a large number of possible trapping sites for electrons or holes at differing energy levels throughout the band gap.[106] Figure 24 (modified from ref 106) shows an early diagram of a number of shallow electron traps detected by various spectroscopies. At least eight electron traps at energies in a region up to 0.87 eV below the conduction band edge are reported in single crystals of rutile. These are assigned to Ti^{3+} interstitial sites associated with oxygen vacancies in the bulk. The electrons from these trap sites can be observed by various methods following thermal excitation into the conduction band.

4.4. Electron and Hole Scavengers on TiO_2 Surfaces

The recombination rate of excited electrons and holes directly affects the reaction rate for any photochemical

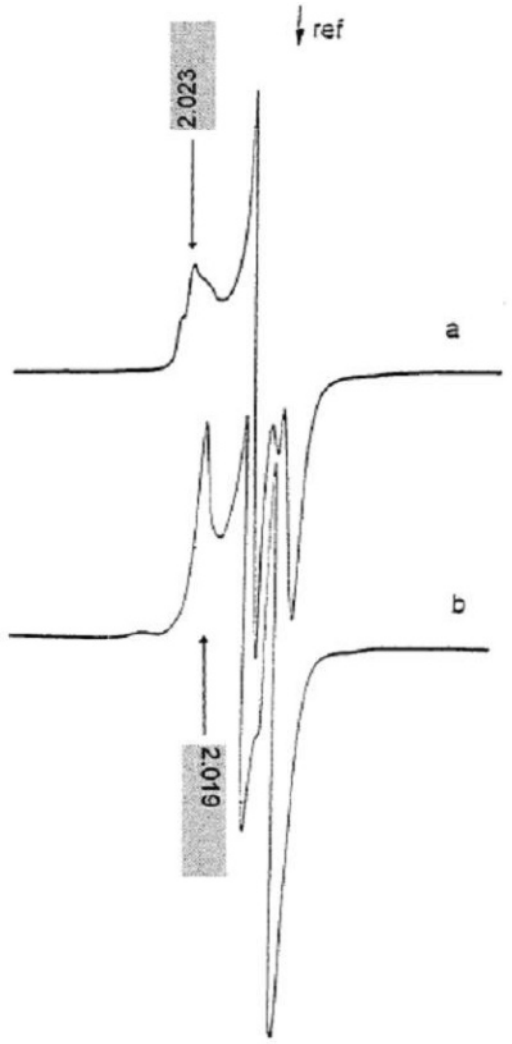

Figure 25. EPR spectra of the O_2^- superoxide ions adsorbed on (a) TiO_2 powder and (b) TiO_2-supported WO_3 powder. Reprinted with permission from ref 92. Copyright 1999 J. G. Baltzer, AG, Science Publishers.

process that occurs on the substrate. The rate of recombination is affected by a number of factors including charge trapping (discussed above), the chemisorption or physisorption of target molecules, and the incident light intensity among others. Often, a sacrificial electron or hole scavenger is used to decrease the recombination rate and, in turn, to increase the lifetime of the other charge carrier. This technique is commonly employed for photochemical systems involving metal oxide semiconductors such as TiO_2.

Perhaps the most referenced electron scavenger used to prolong the lifetime of photogenerated holes is adsorbed molecular oxygen, which readily accepts an electron to become the superoxide ion as discussed by Anpo.[92] Figure 25 shows examples of the detection of the superoxide O^{2-} adsorbed species on (a) TiO_2 powder and (b) TiO_2 supported on WO_3 powder. The spectra in Figure 25 were obtained after a partially reduced TiO_2 surface was exposed to O_2(g) at room temperature. Spectrum a shows a major O_2 resonance at $g_{zz} = 2.023$, with less abundant species exhibiting resonances at $g_{zz} = 2.027$ and 2.020. These three resonances are the result of the absorption of O_2 at different types of Ti^{4+} sites on the TiO_2 surface. Spectrum b was obtained for TiO_2/WO_3 and exhibits a superoxide ion resonance at $g_{zz} = 2.019$.

Using IR absorption spectroscopy, Panayotov et al.[27] and others[79,109] have observed the loss of thermally excited conduction band electrons to adsorbed O_2, forming O_2^-. For photoproduced holes, commonly employed scavenger molecules include methanol,[66,110−114] propanol,[115] ethanol,[112] glycerol,[116] and surface hydroxyl groups.[117]

5. Charge Transfer to Adsorbed Species

Interfacial charge transfer between photoactivated semiconductor surfaces and adsorbate molecules is centrally important to the understanding of photochemical processes. The following section will address the interactions between adsorbed oxygen and TiO_2. In addition, section 5.2 addresses the role of the adsorbate electrophilicity on the efficiency of charge transfer. Although studies of charge transfer effects in the presence of water have important relevance to technologies that operate in aqueous phase, few surface science studies involving well-characterized single crystals operating as photocatalytic substrates under water are available. The work reported in section 6.3.3 is an exception to this generalization, and work reported in section 6.3.1 also deals with the interaction of water with the TiO_2(110) surface.

5.1. Oxygen Chemisorbed on TiO_2 Surfaces

The interaction between adsorbed O_2 and TiO_2 surfaces has been extensively studied on polycrystalline as well as single-crystalline substrates both theoretically[93,94,118] and experimentally.[89,92,119] This section of this review addresses only very recent studies that report on the charge transfer processes that occur between the photoexcited TiO_2 substrate material and the adsorbed O_2 species.

It is well-known that neutral O_2 molecules adsorb as O_2^- on TiO_2 surfaces[92] where electrons are available in the conduction band or from localized Ti^{3+} sites as measured by EPR spectroscopy.[120] Electrons are promoted to the conduction band or to localized Ti^{3+} sites when the sample is reduced (oxygen vacancies are present) or when the sample is activated with UV light above the TiO_2 band gap. Electron transfer from the conduction band to adsorbed O_2 can be monitored using IR spectroscopy,[27] where the decrease in the background IR absorbance is attributed to the loss of conduction band electrons to form the surface O_2^- adsorbate.

5.1.1. Fractal Kinetics for Charge Transport to Chemisorbed Oxygen during Photodesorption

The charge transfer kinetics for photogenerated hole transfer from the surface region of a TiO_2(110) single crystal to an adsorbed O_2 molecule have been studied both experimentally[90,91,121,122] and theoretically[118] using the photodesorption of adsorbed O_2 as a probe of this process. Direct optical absorption of the O_2-TiO_2 adsorbate−surface complex was investigated theoretically.[118] Direct desorption of the O_2^- adsorbate species is found with a maximum in photon energy near 3.7 eV (Figure 26). These calculations are compared with experimental data,[90] showing that excitation and oxygen desorption occur over a broader range of photon energies. Thus, it is postulated that direct photoexcitation is accompanied by hole-mediated desorption of O_2, where the photoproduced hole abstracts an electron from the adsorbed superoxide ion, leading to molecular O_2 desorption.[118]

As discussed in section 4.2, the rate for O_2 photodesorption depends linearly on the square root of the incident light

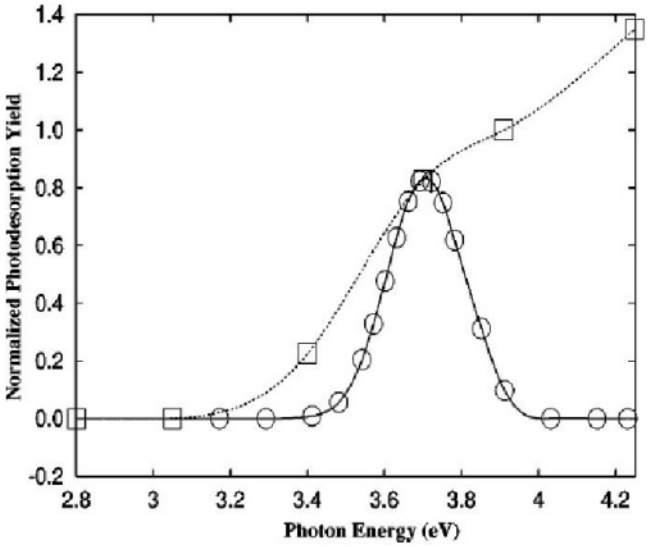

Figure 26. Comparison of theoretical cross section for O_2 photodesorption from TiO_2(110) as a function of photon energy. The dotted curve is from ref 90 and the solid line curve is from the calculation of the direct photodesorption of O_2, with arbitrary scaling. Reprinted with permission from ref 118. Copyright 2003 The American Institute of Physics.

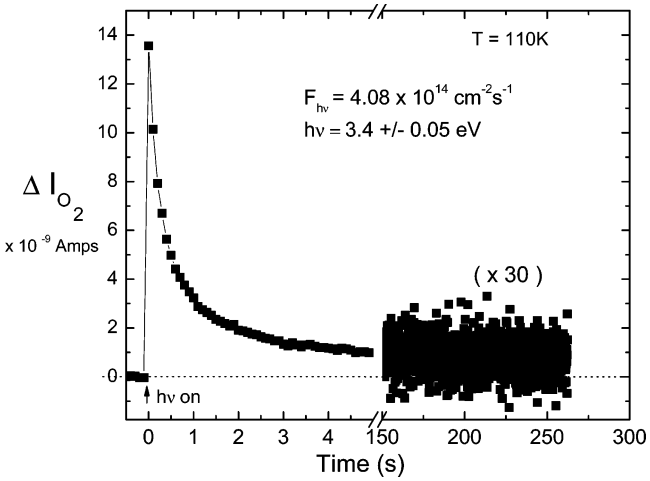

Figure 27. Oxygen photodesorption experiment for O_2 on TiO_2(110). Significant desorption is still measured even after 200 s. Reprinted with permission from ref 123. Copyright 2006 American Chemical Society.

intensity.[66] The O_2 photodesorption process is affected by charge carrier trapping and the subsequent saturation of traps as described.[66] The mechanism for the photodesorption of adsorbed O_2^- from TiO_2(110) is based on the activation of the adsorbed O_2^- by a photogenerated hole that results in the neutralization of the oxygen molecule and, finally, the desorption of the neutral species.[118] The detailed reason for O_2 photodesorption when charge transfer occurs is currently unknown. When continuous UV irradiation is employed as the excitation source, the O_2 photodesorption from TiO_2(110) can be observed over a time scale of hundreds of seconds as shown in Figure 27. Previous work[90,121] has fit the O_2 photodesorption curve to a multiexponential function: the presented model described the presence of three types of adsorbed oxygen species (α_1, α_2, and β), each exhibiting its own cross section for photodesorption. The results presented in refs 66 and 123 have reconsidered this model for photodesorption. The new findings suggest that it is appropriate for the O_2 photodesorption process to be described

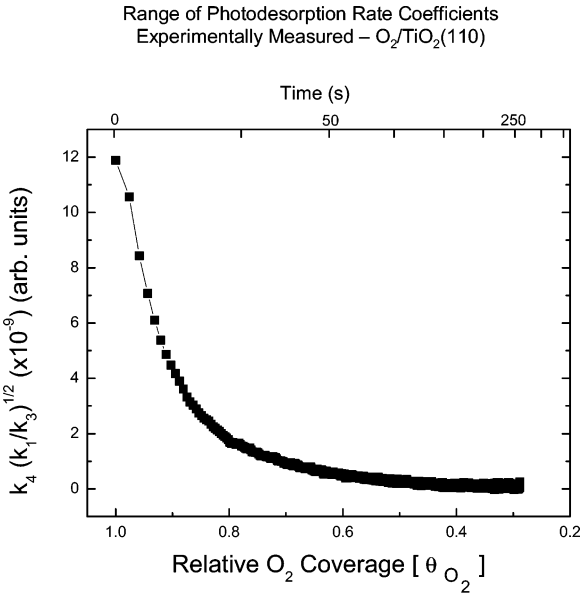

Figure 28. Plot of $k_4(k_1/k_3)^{1/2}$ for the photodesorption of oxygen from TiO_2 as a function of the remaining O_2 coverage. Reprinted with permission from ref 123. Copyright 2006 American Chemical Society.

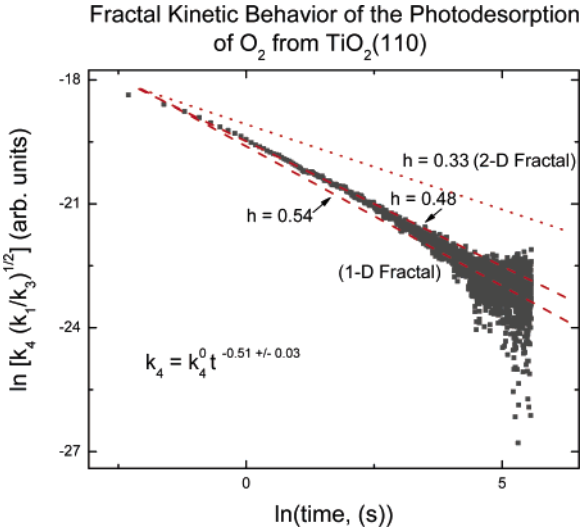

Figure 29. Scaling plot that describes the fractal kinetic behavior for O_2 desorption from TiO_2(110). The scaling factor, *h*, for this fit suggests that electron transport across the TiO_2(110) surface may be one-dimensional. Reprinted with permission from ref 123. Copyright 2006 American Chemical Society.

as a fractal kinetic process, as discussed below and in ref 123.

When one considers the rate of the photodesorption of O_2 from TiO_2(110) according to the equations presented in section 4.2, the following expression can be derived:

$$-\frac{d[\theta_{O_2}]}{dt} = k_4[O_2^-(a)]\left(\frac{k_1}{k_3}\right)^{1/2} F_{h\nu}^{1/2} \qquad (6)$$

In eq 6 the rate of change in the photodesorption of oxygen is related to the product of the rate constants. As shown in Figure 28, the product of the rate constants describing the hole excitation, hole recombination with electrons, and hole transfer to adsorbed O_2^- is plotted against the relative coverage of adsorbed oxygen. The resulting plot depicts a drastic decrease in the rate constant term, $k_4(k_1/k_3)^{1/2}$, by a

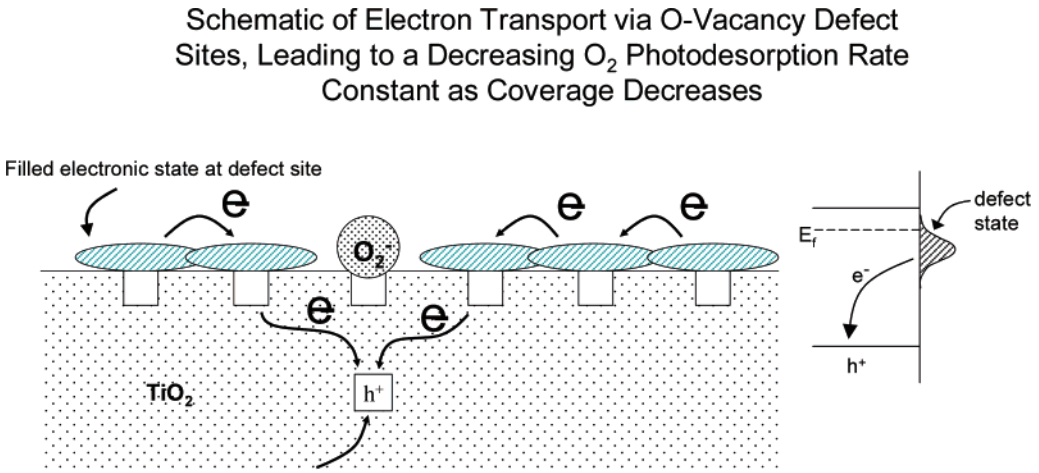

Figure 30. Diagram of the electronic charge clouds associated with surface oxygen vacancy sites on the reduced TiO_2(110) surface. Percolation through the charge clouds at unoccupied vacancies is postulated to be one-dimensional and to lead to recombination with photoproduced holes. Reprinted with permission from ref 123. Copyright 2006 American Chemical Society.

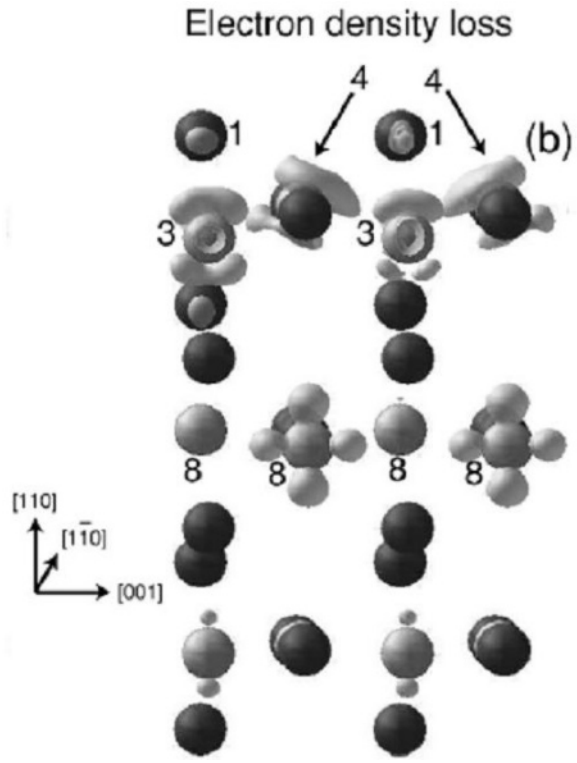

Figure 31. Electron density associated with an O vacancy defect site on TiO_2(110). The electron density lobes represent the decrease of electron density when an O atom is added to the defect site and, hence, the excess electron density initially present at and around the defect. Reprinted with permission from ref 127. Copyright 2003 The American Institute of Physics.

factor in excess of 100 over the time period of the photodesorption measurement. The change in the rate constant term during this experiment can be explained by a fractal rate law, where the rate constant, k_4, varies as a function of coverage. The constants k_1 and k_3 are likely to be unvarying in the experiment, being determined by the solid state properties of the TiO_2 (see section 4.2).

A model for the large decrease in k_4 during the O_2 photodesorption process involving a fractal kinetic rate law is described by Kopelman.[124−126] In a fractal kinetic process, reactions are described with a rate coefficient, as opposed to a rate constant. The rate coefficient varies as the reaction progresses *through time* according to the following equation

$$k_4 = k_4^\circ t^{-h} \tag{7}$$

or

$$\ln k_4 = -h \ln t + const \tag{8}$$

Figure 29 shows a scaling plot used to deduce the fractal character of O_2 photodesorption from TiO_2(110) surfaces, where the exponential coefficient, *h*, used to describe this process is found to be on the order of 0.50. According to Kopelman, the magnitude of *h* provides insight into the dimensionality of the fractal process that occurs on the surface. For values of *h* near 0.50, the fractal percolation process is characterized as being one-dimensional. An alternate view of the origin of the decrease in k_4 observed in these experiments is that there are many different types of sites inside and on the TiO_2 surface that promote electron−hole pair recombination with different efficiencies. This conventional viewpoint of what is happening would probably not yield the linear scaling plot over >2 decades, shown in Figure 29.

Figure 30 schematically represents the postulated one-dimensional electron transport route that occurs across the surface of defective TiO_2(110). The defective TiO_2 surface has excess electrons centered at oxygen vacancies, as described earlier in this review. However, work by Vijay et al.[127] has suggested that the electrons associated with the oxygen vacancy are somewhat delocalized, thus creating a large so-called "charge cloud" of electron density around the vacancy site. Figure 31 shows a plot of the electron density changes that occur upon binding of an O atom at a vacancy site on the TiO_2(110) surface. The vacancy density in the surface is large, 0.5 ML. The electron density loss regions are shown as lobes surrounding the light gray Ti atoms and the dark gray oxygen atoms. It may be seen that when the O atom is added to the vacancy site, electron density is lost from regions rather far removed from the atoms. The electron density is preferentially removed from regions near 6c-Ti atoms (labeled 4) and elsewhere also, such as at position 8. The removal of electron density by the addition of an O atom to a vacancy may be used as evidence for the existence of extra electron density in the vicinity of the defect site. It is noted that the extra electron density

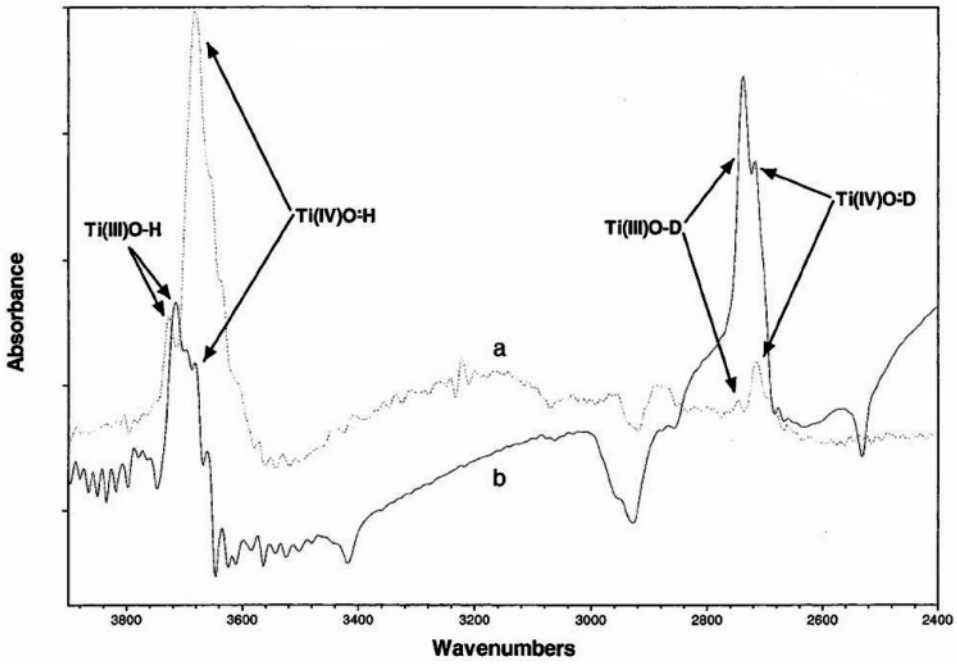

Figure 32. Difference infrared spectra for TiO_2 powder irradiated by UV irradiation. Spectrum a was obtained by subtracting from the spectrum of the irradiated powder under O_2 the spectrum without irradiation. Spectrum b was obtained from the spectrum for the irradiated TiO_2 in vacuum from which the spectrum without irradiation has been subtracted. The hydroxyl stretching regions for Ti−OH and Ti−OD species are shown. Reprinted with permission from ref 79. Copyright 2000 American Chemical Society.

associated with the defect site is highly delocalized about the defect site, a new finding about these spectroscopically observed electronic states.

These charge clouds may interact with one another, providing a network of available routes for charge transfer. The network of filled electronic states at vacancy defect sites is disrupted by O_2 adsorption at these sites. Thus, this network becomes more interconnected as the coverage of oxygen adsorbed at vacancies *decreases* and therefore may serve as electron conduction channels to neutralize photoproduced holes. The fit to this fractal model, shown in Figure 29, suggests that the fractal network is in fact a one-dimensional conductive network. As a result, the value for k_4 will decrease with $h = 0.5$ as the coverage of interconnected charge clouds increases while the photodesorption process proceeds.

5.2. Role of Adsorbate Electrophilicity on Charge Transport

As described in section 3.2.1, infrared spectroscopy can be employed to investigate the excitation of charge from the valence band into the conduction band for TiO_2 and mixed TiO_2-SiO_2 materials. For polycrystalline TiO_2, it has been shown that electrons are trapped in the conduction band upon either thermal or photon excitation, where they reside for long times if the temperature is sufficiently low.[27] The conduction band is depopulated by warming the sample or by charge transfer from the conduction band to adsorbates on the surface.

Panayotov et al.[76] have investigated this charge transfer process on TiO_2-SiO_2 powdered material, where the charge transfer from the conduction band to two different adsorbate molecules is compared. There it was found that efficient charge transfer occurs exclusively between the TiO_2 surface and an adsorbate molecule with an electrophilic moiety. No observable charge transfer occurred with a similar molecule

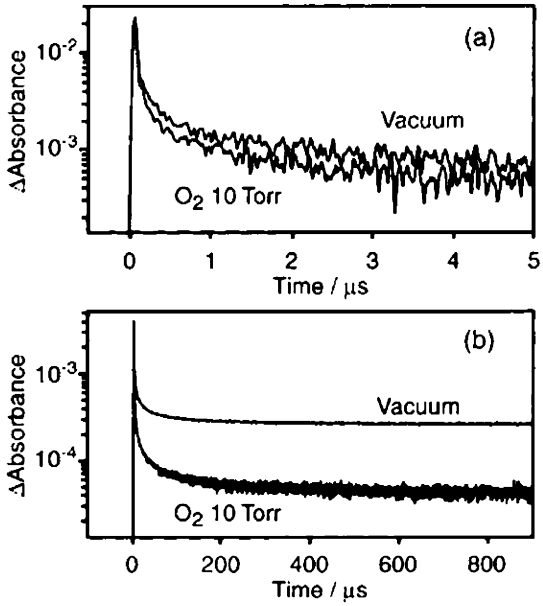

Figure 33. Transient IR absorption intensity observed on TiO_2 powder irradiated by a 355 nm laser pulse. Two response curves are shown in vacuum and in the presence of O_2(g) on two time scales, and the influence of adsorbed O_2 on the decay kinetics is evident. Reprinted with permission from ref 128. Copyright 2001 American Chemical Society.

with the electrophilic moiety removed. The adsorbate molecules employed for this work were 2-chloroethyl ethyl sulfide (2-CEES) and diethyl sulfide (DES). These molecules have the same chemical structure, except that the 2-CEES molecule has a chlorine atom on one terminus of the molecule. The charge transfer processes measured in that work are recorded as a change in the level of IR background absorbance, which is directly related to the concentration of trapped electrons in the conduction band of the TiO_2-SiO_2 mixed oxide. Figure 34 shows the change in the background

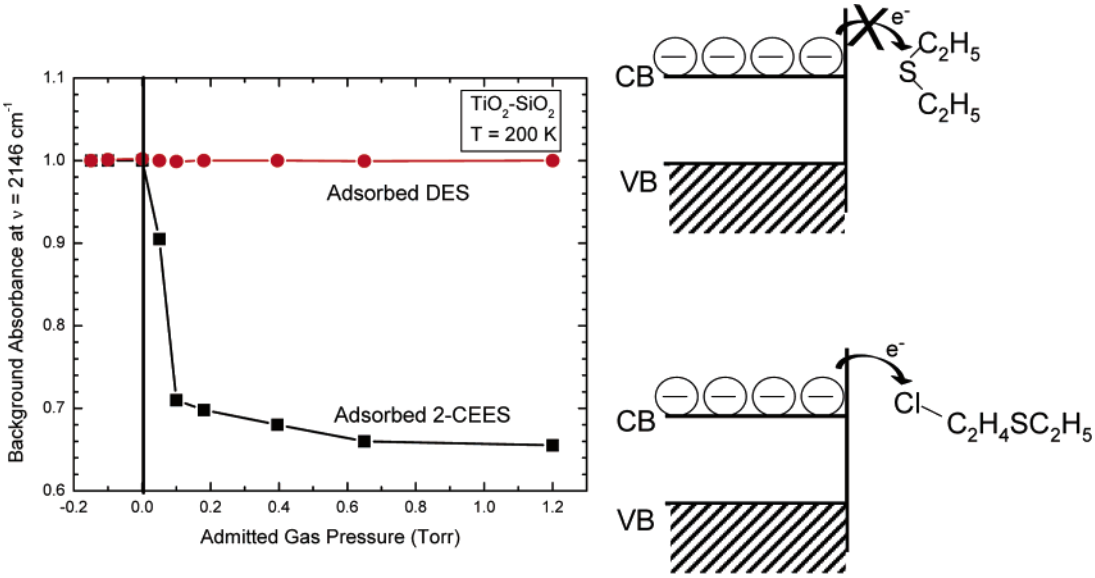

Figure 34. Preferential charge transfer from the conduction band of TiO_2 (in $TiO_2 - SiO_2$) to molecules adsorbed through an electrophilic moiety. Reproduced in part from Reference.[76] Copyright 2003 Elsevier B. V.

IR absorbance versus the pressure of the admitted adsorbate gas. For the 2-CEES molecule, a clear decrease in the concentration of trapped electrons in the conduction band is observed as efficient charge transfer occurs from the substrate to the adsorbate. For adsorbed DES, no change in the level of trapped electrons is observed. The authors attribute this effect to the large electronegativity of the chlorine atom[76] and to direct electron transfer to the Cl atom in the molecule. Similar effects were also observed by Hoffmann et al.[79,80] and Yamakata et al.[128] In Figure 32, infrared spectra are presented in which the −OH and −OD spectral regions for adsorbed hydroxyl groups are shown. The highly magnified difference spectra show that a blue shift occurs for both isotopomers when Ti(III) sites, bonded to OH or OD groups, are oxidized to Ti(IV) sites by O_2(g) while being irradiated by UV light. These results suggest that the hydroxyl stretching frequency can be used as a diagnostic for the dissociation of O_2 on oxygen-vacancy defect sites, which are filled by O_2 adsorption.[79]

In Figure 33, Yamakata et al.[128] have shown, in transient kinetic measurements of the decay of the infrared background signal due to conduction band electrons, that the presence of O_2(g) enhances the decay kinetics, particularly for the portion of the kinetics observed in the 10−100 μs regime of decay kinetics. This effect is ascribed to the production from O_2(a) of superoxide surface ions using excited electrons, that is, to transport of conduction band electrons to the surface to encounter O_2 electron scavenger molecules.[128]

Panayotov et al.[129] also later investigated the same effect with TiO_2 as the substrate material rather than the TiO_2−SiO_2 mixed oxide. In that work, the same effect is measured. For both 2-CEES and ethyl chloride (not shown), efficient electron transfer occurs from trapped electrons in the conduction band to the Cl atom in the adsorbate molecule. Adsorbed DES does not accept electrons from the conduction band of the TiO_2. Upon charge transfer from the conduction band to either 2-CEES or ethyl chloride, ethoxy groups are formed as the reduction product for the charge transfer process.[129]

6. UV-Induced Hydrophilicity of TiO_2

6.1. Introduction

In addition to the photo-oxidative effect observed on TiO_2 surfaces and in suspensions of TiO_2 colloids, TiO_2 surfaces have been more recently studied with the aim to understand the UV-induced hydrophilicity effect first reported by Wang et al. in *Nature*.[5] Figure 35 shows the extraordinary wetting effect observed for water droplets contacting a polycrystalline

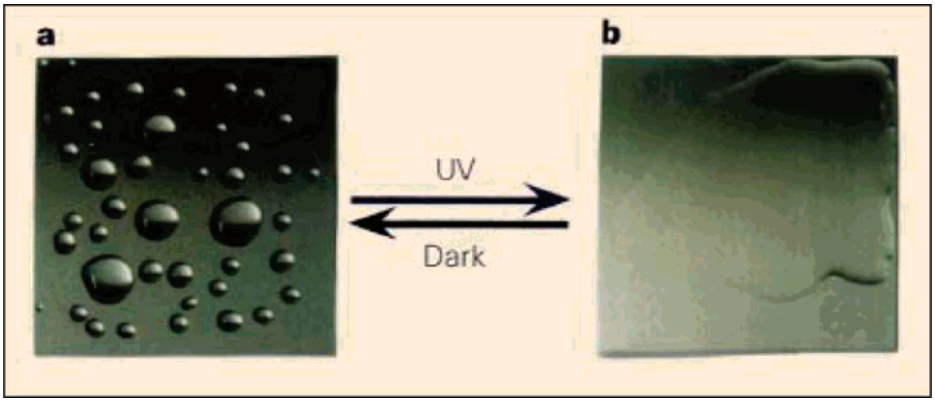

Figure 35. (a) Hydrophobic TiO_2 film surface before UV irradiation in air; (b) hydrophilic TiO_2 film surface after irradiation with UV light. Reprinted with permission from *Nature* (http://nature.com), ref 5. Copyright 1997 Nature Publishing Group.

TiO_2 film deposited from a colloidal suspension of anatase particles on a glass substrate, which was then annealed in air at 773 K.[5]

In that paper, it was shown that the wettability of TiO_2 surfaces studied under ambient atmospheric conditions is controlled by exposure to UV light, where an apparent contact angle of the pre-irradiated TiO_2 surface was measured to be ~72°. After irradiation, angles of 0−1° were reported. This study investigated both polycrystalline films and single-crystal (rutile and anatase) samples, thus concluding that the observed UV-induced hydrophilicity was an inherent property of TiO_2 and did not change on the basis of the character of the specific type of TiO_2 material. In that work,[5] Wang et al. propose that the UV light generates oxygen vacancies which were postulated to be active sites for water dissocation. The single-crystal TiO_2 surface was observed to be composed of both hydrophilic and hydrophobic domains (microscopic in size) as measured using frictional force microscopy. The authors proposed that the hydrophilic domains dominate the overall macroscopic interaction between the surface and the macroscopic water droplet. One year later, the same authors published a full paper including additional measurements yet still proposing the same UV-induced defect model (production of surface Ti^{3+} ions by UV).[6] In that work, the authors report evidence of the production of both hydrophilic and oleophilic domains in agreement with their earlier work. The hydrophilic domains are attributed to defect sites where dissociative water adsorption occurs, and the physical reason for the development of domain structures was unexplained. The remainder of the surface is said to be oleophilic. However, the authors did recognize that hydrocarbon layers are measurable contaminants on the surface of the TiO_2 films, which they investigated, but they claim the hydrophilicity effect on TiO_2 is governed by UV-induced defect production. Photo-oxidation of hydrocarbons present in their experiments in the ambient atmosphere is considered by those authors to be an independent process unrelated to UV-induced hydrophilicity.[6]

Since the publication of those early papers,[5,6] a large amount of work has been done to elucidate the mechanism for the UV-induced hydrophilicity effect. Until recently, when the mechanism was clearly defined by workers in this laboratory,[130] this effect has been debated and a number of mechanisms have been proposed, most of which will be discussed in the next section. However, even without a clear understanding of this phenomenon, a large number of commercial products have been developed based on this technology, including windows and mirrors that are self-cleaning and anti-fogging. As a result, this area of metal oxide surface photochemistry has generated broad interest.

Below, we address the most commonly used techniques for measuring hydrophilic effects on TiO_2 and review a number of proposed mechanisms and experiments found in the literature. In addition, some very recent experimental results clarifying the dominant mechanism of photoinduced hydrophilicity will be presented.

6.2. Contact Angle Measurements

The most commonly employed and direct method for measuring surface hydrophilicity or hydrophobicity is though analysis of the water contact angle. Contact angle measurements are most simply done using the sessile drop method, which has been extensively reviewed by Neumann and Good[131] and is briefly explained here. The sessile drop method involves the placement of a droplet of liquid onto a horizontal surface and measuring the contact angle, either directly or through analysis of a digital image of the droplet on the surface. The solid−liquid interaction at the surface obeys Young's equation as

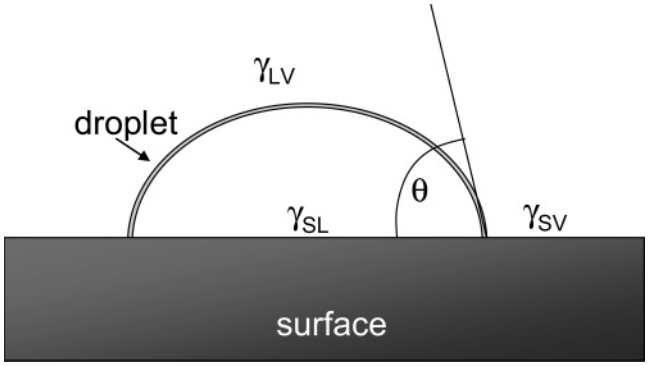

Figure 36. Diagram of the vector forces present at the solid−liquid interface. The measured contact angle (θ) is shown.

$$\gamma_{LV} \cos \theta = \gamma_{SV} - \gamma_{SL} \quad (9)$$

where γ_{LV} is the surface tension between the interface between the water droplet and the surrounding atmosphere, γ_{SV} is the surface tension between the surface and the surrounding atmosphere, γ_{SL} is the surface tension between the surface and the liquid, and θ is the contact angle as shown in Figure 36. At the three-phase interface, the vector forces balance is described by eq 9. The measurement of droplet contact angles on a surface often involves a large variability of reported angles, and such measurements should be considered as qualitative indicators that may vary drastically with experimental conditions, including atmospheric humidity, surface and/or droplet contamination, among others.[132] Additionally, contact angle measurements below 10°, signifying a super-hydrophilic surface, are especially hard to analyze due to the inability to measure such low contact angles.

Reported contact angle measurements on titania surfaces have traditionally used a method that involves pre-irradiation of the surface in ambient air, followed by droplet placement on the surface and then contact angle measurement. The general consensus of a great deal of work done by a number of different groups[133−140] using this experimental protocol is that a gradual decrease in the measured contact angle occurs with increasing pre-illumination time in the air. Representative results are shown in Figure 37. Here, pre-irradiation of the anatase films with three UV irradiation intensities (0.2−1.0 mW/cm^2) is employed followed by water contact angle measurements in the air. A monotonic decrease in contact angle is measured as the irradiation time is increased, terminating at contact angles between 5° and 10°.[137]

An experimental study,[130] described in a later section, uses a technique that involves direct UV irradiation *during* contact angle measurement and records consecutive digital images thus enabling one to watch in real time the contact angle changes with increasing UV illumination time. The use of this method for contact angle analysis has shown surprisingly that *sudden wetting* occurs at a critical UV exposure time. The in situ method shows an instantaneous wetting of the TiO_2 surface by the water droplet after some critical time period for UV illumination.[130] Further details of these

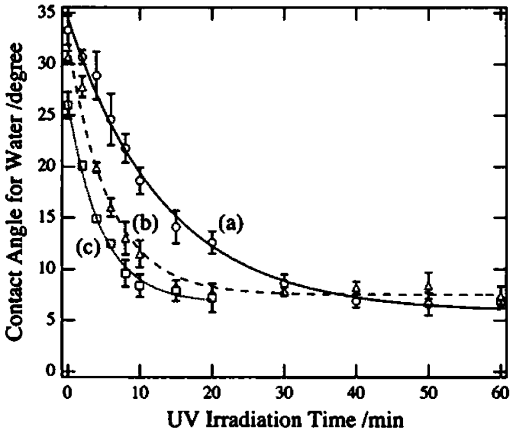

Figure 37. Changes of the contact angle for water on a TiO_2 film following irradiation with UV radiation in ambient air at three power densities: (a) 0.2 mW cm^{-2}; (b) 0.7 mW cm^{-2}; (c) 1.0 mW cm^{-2}. Reprinted with permission from ref 137. Copyright 2003 American Chemical Society.

measurements will be presented in section 7.3.3. In contrast, all contact angle measurements made in ambient air show a gradual decrease in contact angle with increasing irradiation time, and this effect is attributed to the occurrence of continuous contamination of the surface by hydrocarbon molecules present at parts per million levels in the ambient air, making such measurements ineffective for mechanistic studies of the origin of the hydrophilicity effect.

6.3. Proposed Models

From the survey of the massive amount of literature dealing with the UV-induced hydrophilicity effect on TiO_2 surfaces, three possible mechanisms have been proposed as discussed below.

6.3.1. UV-Induced Defect Production

First proposed by Wang et al.[5,6] at the time of the discovery of the photoinduced wetting effect, this model involves the production of Ti^{3+} ions at the surface as a result of oxygen atom ejection from the lattice. This model has since been also proposed by a number of additional authors.[133−136,141] The defects, known as oxygen vacancies or Ti^{3+} sites, when produced on the surface by thermal activation are known to cause water dissociation[29−31] and, thus, the production of adsorbed −OH species, which are known to be hydrophilic in nature. As a result, this was a first logical explanation for the UV-induced hydrophilicity effect.

The UV-induced defect formation postulate was directly and quantitatively investigated, and results have been reported by Mezhenny et al.[42] In that work, the STM was used to probe TiO_2(110) surfaces which have been irradiated extensively with known fluxes of 1.6−5.6 eV of UV photons under atomically clean conditions in ultrahigh vacuum. Both the (1 × 1) and (1 × 2) surfaces were investigated both before and after UV irradiation. The result of this study was starkly conclusive. For the (1 × 1) surface, statistical counting of defect sites present on the surface revealed that ***no*** additional defects are formed with UV irradiation ($h\nu \geq$ 3.0 eV) with $>5 \times 10^{24}$ photons cm^{-2}. Figure 38 shows representative STM images of the TiO_2 surface before UV irradiation and after UV exposure to $>5 \times 10^{24}$ photons cm^{-2}. Statistical counting of oxygen vacancies (imaged as bright spots) revealed no statistically significant difference

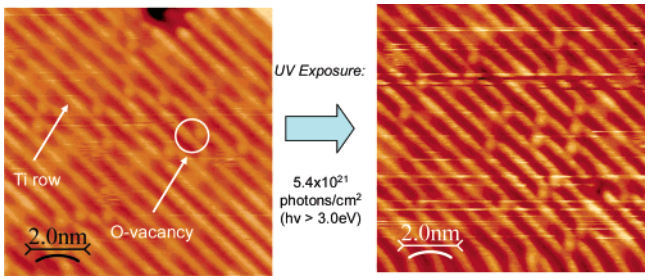

Figure 38. STM images of the partially reduced TiO_2(110)−(1 × 1) surface before and after UV irradiation. No additional defect formation is observed as a result of UV irradiation, negating the proposed UV-induced hydrophilicity model that suggests otherwise. Reprinted with permission from ref 42. Copyright 2003 Elsevier B.V.

in the vacancy defect concentration before or after UV illumination for these very high irradiation fluences. For the (1 × 2) surface, which is produced by high-temperature thermal annealing,[9] the *upper limit* of the cross section for defect formation was measured to be on the order of $10^{-23.5} \pm 0.2$ cm^2. The highly reduced (1 × 2) surface is not representative of a TiO_2 surface in ambient conditions. This demonstrated insensitivity of TiO_2(110) to UV irradiation indicates that, using the average power levels reported in the literature for the UV-induced hydrophilicity effect to be seen, one would have to irradiate a TiO_2 surface for many days to produce the defect density necessary to cause a macroscopic change in the wetting characteristics of the surface. This work therefore provides conclusive evidence at the atomic level that the UV-induced defect formation postulate is incorrect. In addition, recent DFT calculations presented by Bouzoubaa et al.[142] show the energy of formation of an O vacancy defect to be on the order of ∼7 eV for rutile surfaces, confirming that UV irradiation at significantly lower photon energies cannot be responsible for vacancy formation. In the theoretical studies of Bouzoubaa et al.,[142] the ∼7 eV formation energy for an O vacancy defect is calculated by assuming that an O(^{3}P) atom is generated photochemically. If, instead, half of a ground state O_2(g) molecule were generated, the vacancy formation energy would decrease to ∼4.5 eV, also precluding the possibility of UV-induced vacancy formation in causing the hydrophilicity effect on TiO_2.

A second study, carried out on TiO_2(110), has also contradicted the concept that O vacancy defects somehow cause the surface to become hydrophobic. Here, Henderson and co-workers[143] have compared the thermal desorption kinetics for adsorbed water on TiO_2(110) in the absence of O vacancy defects and under conditions where the defects have been produced by controlled annealing in vacuum at 850 K for 10 min. It was found that the desorption kinetics for undissociated H_2O on the two surfaces were essentially identical, both for the first monolayer and for subsequent monolayers. This indicates that the binding energy of H_2O molecules is not influenced by the presence of about 13% defect sites in the annealed surface, whether the H_2O is adsorbed in the first or subsequent monolayers. Because the contact angle between H_2O molecules and the surface is governed by the surface energy, this result indicates that the contact angle will not be influenced by defect sites, contrary to the conclusions of Fujishima and Hashimoto and their colleagues.[5,6,133−136,141] The model invoking surface defects fails as a result of two key surface science observations: (1) Surface defects are not produced by UV irradiation, and (2)

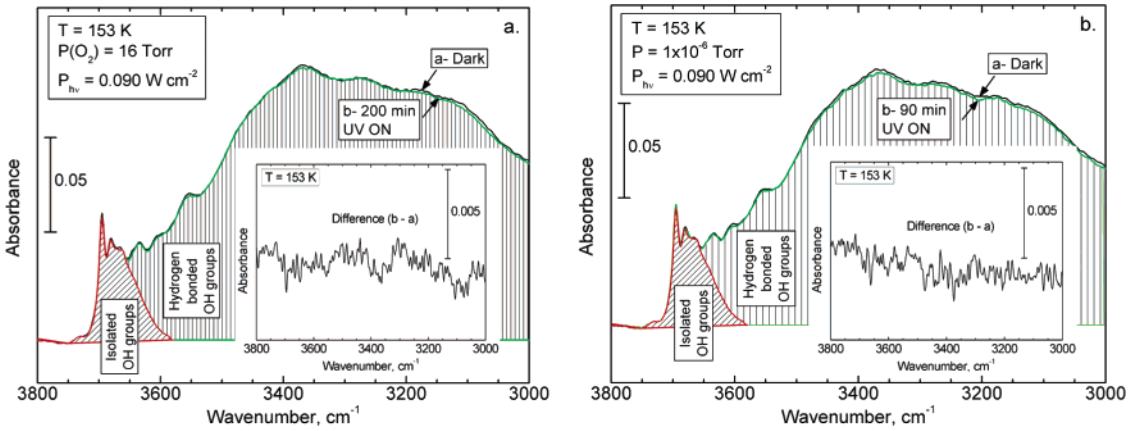

Figure 39. IR absorption spectra for −OH groups on TiO_2 both before and after UV irradiation in O_2 and in vacuum. No observed change in the spectrum due to OH groups is measured. Reprinted with permission from ref 130. Copyright 2005 American Chemical Society.

surface defects produced by controlled thermal annealing do not affect the interaction energy between H_2O molecules and the surface. In the work of White et al.[143] it was shown that H_2O molecules dissociate at the defect sites, but the hydroxylation does not change the interaction energy with subsequently adsorbed water molecules.

6.3.2. UV-Induced Rupture of Ti–OH Bonding

A second model proposed by Sakai et al. in 2003[137] suggests that the UV-induced hydrophilicity effect is due to surface modifications, which, in the presence of H_2O, lead to an increased surface coverage of Ti−OH groups. This model was proposed on the basis of XPS, IR, and electrochemical measurements. The authors explain this effect in the following way: −OH groups that are bound in 2-fold coordination to Ti atoms are converted by H_2O adsorption into two −OH groups that are singly coordinated each to their own Ti atom. Further XPS investigations done by Gao et al.[144] suggest a similar mechanism, where Ti−OH groups are converted into Ti−OH groups that are associated with dangling bonds.

Experiments have now been done which suggest that the mechanisms suggested in refs 137 and 144 are invalid.[130] These experiments involve the use of a powdered TiO_2 sample that has been exposed to UV light under high-vacuum conditions to study how UV light affects chemisorbed H_2O or Ti−OH bonds found on the TiO_2 surface. IR measurements were made after 200 min of sample irradiation ($h\nu$ = 3.82 eV, 1.76×10^{21} photons cm^{-2}), and no spectral changes were observed in the 3800−3000 cm^{-1} hydroxyl-stretching region, suggesting that no changes occur in the surface-bonding character of Ti−OH groups and of adsorbed H_2O molecules due to UV illumination.[130] These spectroscopic measurements are shown in Figure 39. These experiments were done on a cooled TiO_2 sample (T = 153 K) to avoid heating by the UV lamp.

6.3.3. Photo-oxidation of Hydrophobic Contaminant Layers

A third model for the UV-induced hydrophilicity effect on TiO_2 simply involves the removal of a hydrophobic hydrocarbon monolayer by photo-oxidation. The atomically clean TiO_2 surface produced is hydrophilic.

Work done by Wang et al.[145] has employed sum frequency generation (SFG) as a surface-sensitive technique to investigate wettability effects on nanoparticulate anatase TiO_2 films. This work notes that the as-prepared surface, while appearing to be clean when investigated using Fourier transform infrared spectroscopy (FTIR), contains trace hydrocarbon layers as measured using SFG as would be expected in any experiment conducted in an ambient atmosphere. Although not proven directly, these authors suggest that the UV-induced photocatalytic removal of hydrocarbons is the explanation for the wettability effect.

The photocatalytic removal of adsorbed hydrocarbons was first postulated as the *sole cause* for the hydrophilicity effect on TiO_2 in 2003.[144,146] However, no firm experimental proof has verified this postulate until recently. Zubkov et al.[130] directly investigated the UV-induced wettability phenomenon through careful study of an atomically clean rutile (110) single-crystal surface, prepared in ultrahigh vacuum followed by surface characterization (Auger spectroscopy and LEED) and then exposure to a water droplet for contact angle measurements in situ, under highly controlled atmospheric purity conditions. The ultrahigh-vacuum system used was designed especially for these measurements on a TiO_2(110) crystal and utilized a preparation and analysis chamber, connected to a pressurizable ultrahigh-vacuum experimental chamber (used for water droplet measurements) through a sliding seal as shown in Figure 40. Included in the design of the atmospheric chamber is a special noncontaminating syringe inlet for deposition of a droplet of highly purified water. The overpressure in the chamber keeps airborne contaminants from entering the chamber as the water droplet is deposited on the surface by a syringe needle injected through a small open tube. The chamber is pressurized with a slight overpressure of 99.9999% pure oxygen gas, which was saturated with purified H_2O vapor. During some experiments, known quantities of *n*-hexane in the parts per million range were added to simulate typical hydrocarbon contamination levels in an ambient atmosphere. As a result, this approach eliminates all potential contaminants that may have had a drastic effect in all experiments performed in ambient air as presented previously in the literature. The method then quantitatively adds known levels of hydrocarbon to observe the effect on the UV-induced wettability of the TiO_2(110) surface.

In the studies conducted by Zubkov et al., contact angle measurements on an atomically clean TiO_2(110) surface were carried out using controlled parts per million levels of a model hydrocarbon, *n*-hexane, to artificially contaminate the

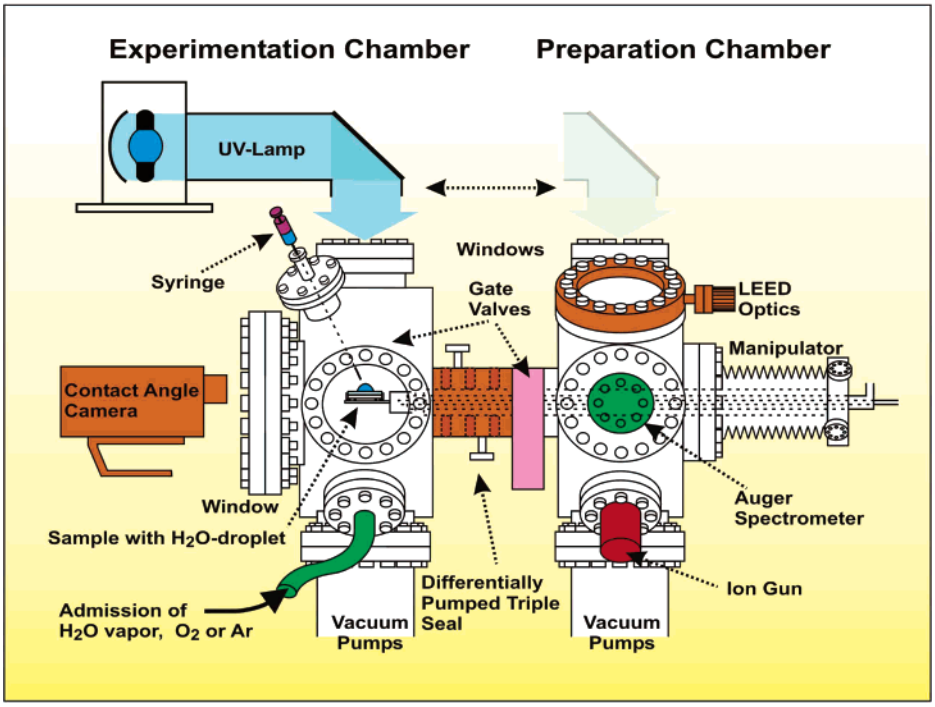

Figure 40. Diagram of the apparatus used for in situ measurements of the water contact angle on TiO_2(110) during UV radiation. Reprinted with permission from ref 130. Copyright 2005 American Chemical Society.

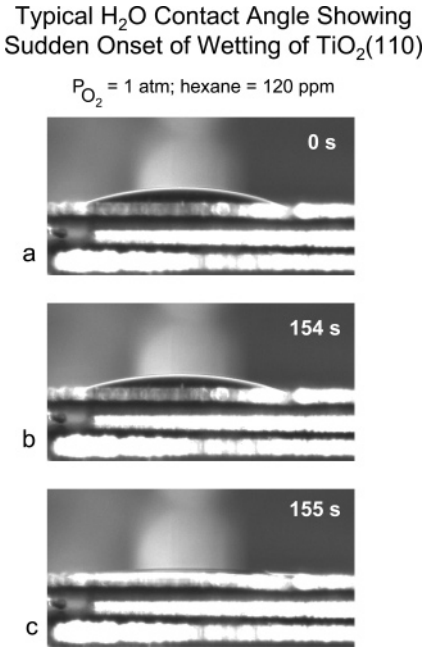

Figure 41. (a) Water droplet on un-irradiated TiO_2 in mixed O_2 + hexane atmosphere; (b) the same water droplet after 154 s of UV exposure; (c) sudden and complete wetting of the water droplet on the TiO_2 surface after 155 s. Reprinted with permission from ref 130. Copyright 2005 American Chemical Society.

surface. In Figure 41, it is shown that upon droplet introduction to the TiO_2(110) surface in an atmosphere consisting of 1 atm of pure O_2(g) and 120 ppm of hexane, a contact angle of ~21° is measured. After irradiation for up to 154 s, the contact angle remains essentially unchanged.

At 155 s, the water droplet suddenly wets the surface, resulting in a contact angle below 10°. The same experiment was done using varied parts per million atmospheric concentrations of hexane in O_2 exposed to the surface. At zero hexane exposure, upon irradiation, the droplet wets the surface almost immediately. A strong correlation between the steady state coverage of adsorbed hexane in equilibrium with gaseous hexane and the irradiation time required for sudden droplet wetting is found, demonstrating the dominant role of hydrocarbon contamination. Data for various levels of hexane exposure are shown in Figure 42, where one can see, in each case, evidence for sudden wetting after a finite induction time that is proportional to the hexane concentration in O_2 at 1 atm.

In these experiments at 300 K, the hexane gas is in equilibrium with adsorbed hexane in a single monolayer, producing a steady state hexane coverage. When UV-induced photo-oxidation of the transient layer of adsorbed hydrocarbon occurs, the equilibrium is disturbed by increasing the rate of loss of adsorbed hexane due to photo-oxidation, and the hexane coverage in the unwet regions of the crystal slowly decreases. At the point where the coverage of adsorbed hexane reaches a critical value near zero monolayers, droplet wetting suddenly occurs. A schematic picture of this effect is shown in Figure 43. In this model, the hydrocarbon layer under the droplet is more slowly oxidized because of screening of this interfacial region from O_2 by the droplet.

These experiments support a model for the UV-induced hydrophilicity effect on TiO_2 surfaces in which the photo-oxidation of adsorbed organic contaminants is the dominant factor leading to a hydrophilic surface.

7. Summary and Outlook

This review has selectively dealt with a number of topics having to do with the photoexcitation of TiO_2, emphasizing recent measurements and theory that are based on modern methods of investigation. In most cases, we have connected what has been discovered by physical measurement of the photoexcitation of TiO_2 to its photochemical behavior. At

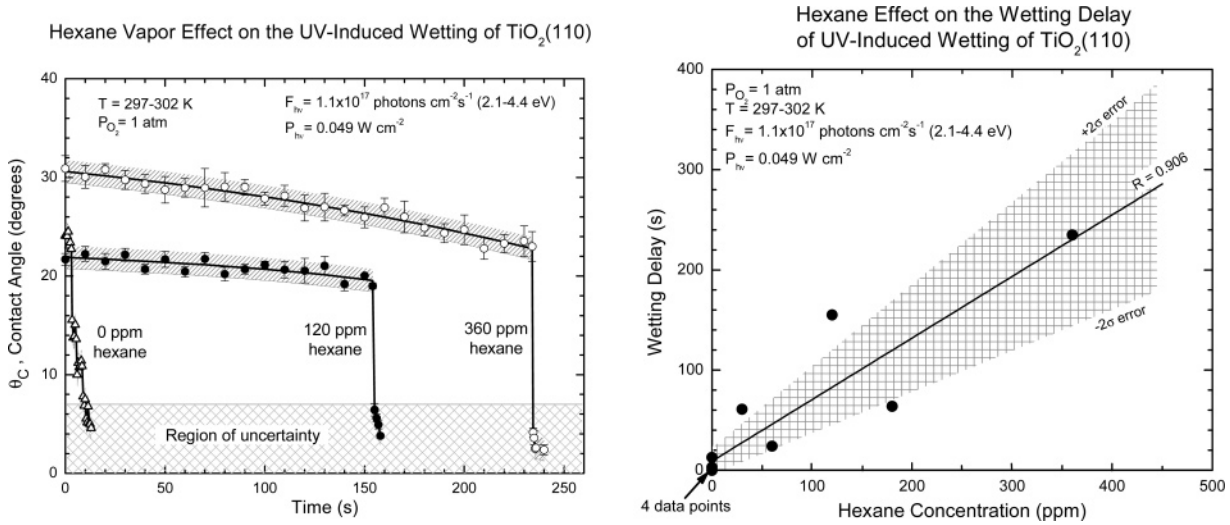

Figure 42. Measured contact angles for water droplets on the TiO_2 surface exposed to various levels of hexane. The induction period before complete wetting increases with increasing hexane partial pressure. Reprinted with permission from ref 130. Copyright 2005 American Chemical Society.

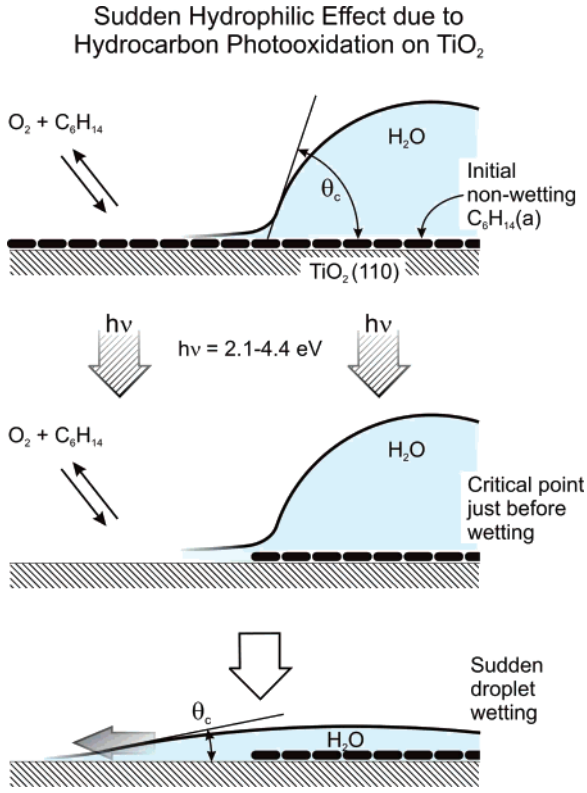

Figure 43. Diagram showing the mechanism for the measured photoinduced hydrophilicity effect on TiO_2 surfaces. Reprinted with permission from ref 130. Copyright 2005 American Chemical Society.

the present time, we are just entering a stage of understanding the photoexcitation of TiO_2 which is beginning to connect to well-known principles of semiconductor physics, based on modern theory and modern surface science experiments at the atomic level of resolution. It is apparent that rather amazing technological developments using the photoexcitation of TiO_2 have moved far beyond our basic understanding of the electronic and chemical processes which occur when TiO_2 is excited by light. It is likely that the rapid growth of research on this topic will continue as new TiO_2-based technologies stimulate the field.

8. Acknowledgments

We thank a number of colleagues, friends, and co-workers for their invaluable suggestions and discussions: Professor Hvorje Petek, Dr. Oliver Diwald, Dr. Tykhon Zubkov, Professor Clemens Burda, Dr. Cristiana Di Valentin, Professor Horia Metiu, and Dr. Mitko Panayotov. We also thank Peter Maksymovych for help with figure design and for STM images. We acknowledge with thanks the support of this work by the DoD Multidisciplinary University Research Initiative (MURI) program administered by the Army Research Office under Grant DAAD 19-01-0-0619.

9. References

(1) Grätzel, M. *Nature* **2001**, *414*, 338.
(2) Grätzel, M. *J. Photochem. Photobiol. C* **2003**, *4*, 145.
(3) Hagfeldt, A.; Grätzel, M. *Chem. Rev.* **1995**, *95*, 49.
(4) Fujishima, A.; Hashimoto, K.; Watanabe, H. *TiO_2 Photocatalysis: Fundamentals and Applications*; BKC, Inc.: Tokyo, Japan, 1997.
(5) Wang, R.; Hashimoto, K.; Fujishima, A.; Chikuni, M.; Kojima, E.; Kitamura, A.; Shimohigoshi, M.; Watanabe, T. *Nature* **1997**, *388*, 431.
(6) Wang, R.; Hashimoto, K.; Fujishima, A.; Chikuni, M.; Kojima, E.; Kitamura, A.; Shimohigoshi, M.; Watanabe, T. *Adv. Mater.* **1998**, *10*, 135.
(7) Sunada, K.; Kikuchi, Y.; Hashimoto, K.; Fujishima, A. *Environ. Sci. Technol.* **1998**, *32*, 726.
(8) Linsebigler, A. L.; Lu, G. Q.; Yates, J. T., Jr. *Chem. Rev.* **1995**, *95*, 735.
(9) Diebold, U. *Surf. Sci. Rep.* **2003**, *48*, 53.
(10) Hasiguti, R. R. *Annu. Rev. Mater. Sci.* **1972**, *2*, 69.
(11) Henrich, V. E.; Cox, P. A. *The Surface Science of Metal Oxides*; Cambridge University Press: Cambridge, U.K., 1994.
(12) *Photocatalysis: Fundamentals and Applications*; Serpone, N., Pilezzetti, E., Eds.; Wiley-Interscience: New York, 1989.
(13) Swamy, V.; Muscat, J.; Gale, J. D.; Harrison, N. M. *Surf. Sci.* **2002**, *504*, 115.
(14) Charlton, G.; Howes, P. B.; Nicklin, C. L.; Steadman, P.; Taylor, J. S. G.; Muryn, C. A.; Harte, S. P.; Mercer, J.; McGrath, R.; Norman, D.; Turner, T. S.; Thornton, G. *Phys. Rev. Lett.* **1997**, *78*, 495.
(15) Lindsay, R.; Wander, A.; Ernst, A.; Montanari, B.; Thornton, G.; Harrison, N. M. *Phys. Rev. Lett.* **2005**, *94*, *246102*.
(16) Thompson, T. L.; Diwald, O.; Yates, J. T., Jr. *J. Phys. Chem. B* **2003**, *107*, 11700.
(17) Lu, G. Q.; Linsebigler, A.; Yates, J. T., Jr. *J. Phys. Chem.* **1994**, *98*, 11733.
(18) Pétigny, S.; Mostéfa-Sba, H.; Domenichini, B.; Lesniewska, E.; Steinbrunn, A.; Bourgeois, S. *Surf. Sci.* **1998**, *410*, 250.
(19) Pan, J. M.; Maschhoff, B. L.; Diebold, U.; Madey, T. E. *Abstr. Pap. Am. Chem. Soc.* **1991**, *202*, 172.

(20) Pan, J. M.; Maschhoff, B. L.; Diebold, U.; Madey, T. E. *J. Vac. Sci. Technol. A* **1992**, *10*, 2470.
(21) Diebold, U.; Lehman, J.; Mahmoud, T.; Kuhn, M.; Leonardelli, G.; Hebenstreit, W.; Schmid, M.; Varga, P. *Surf. Sci.* **1998**, *411*, 137.
(22) Fischer, S.; Munz, A. W.; Schierbaum, K. D.; Göpel, W. *Surf. Sci.* **1995**, *337*, 17.
(23) Wang, L. Q.; Baer, D. R.; Engelhard, M. H. *Surf. Sci.* **1994**, *320*, 295.
(24) Wang, L. Q.; Baer, D. R.; Engelhard, M. H.; Shultz, A. N. *Surf. Sci.* **1995**, *344*, 237.
(25) Göpel, W.; Anderson, J. A.; Frankel, D.; Jaehnig, M.; Phillips, K.; Schäfer, J. A.; Rocker, G. *Surf. Sci.* **1984**, *139*, 333.
(26) Li, M.; Hebenstreit, W.; Diebold, U.; Tyryshkin, A. M.; Bowman, M. K.; Dunham, G. G.; Henderson, M. A. *J. Phys. Chem. B* **2000**, *104*, 4944.
(27) Berger, T.; Sterrer, M.; Diwald, O.; Knözinger, E.; Panayotov, D.; Thompson, T. L.; Yates, J. T., Jr. *J. Phys. Chem. B* **2005**, *109*, 6061.
(28) Kingsbury Jr., P. I.; Ohlsen, W. D.; Johnson, O. W. *Phys. Rev.* **1968**, *175*, 1091.
(29) Henderson, M. A. *Langmuir* **1996**, *12*, 5093.
(30) Henderson, M. A. *Surf. Sci.* **1998**, *400*, 203.
(31) Epling, W. S.; Peden, C. H. F.; Henderson, M. A.; Diebold, U. *Surf. Sci.* **1998**, *412*−*413*, 333.
(32) Bikondoa, O.; Pang, C. L.; Ithnin, R.; Muryn, C. A.; Onishi, H.; Thornton, G. *Nat. Mater.* **2006**, *5*, 189.
(33) Wendt, S.; Schaub, R.; Matthiesen, J.; Vestergaard, E. K.; Wahlström, E.; Rasmussen, M. D.; Thostrup, P.; Molina, L. M.; Laegsgaard, E.; Stensgaard, I.; Hammer, B.; Besenbacher, F. *Surf. Sci.* **2005**, *598*, 226.
(34) Schaub, R.; Thostrup, R.; Lopez, N.; Laegsgaard, E.; Stensgaard, I.; Norskov, J. K.; Besenbacher, F. *Phys. Rev. Lett.* **2001**, *87*, 266104.
(35) Schaub, R.; Wahlstrom, E.; Ronnau, A.; Laegsgaard, E.; Stensgaard, I.; Besenbacher, F. *Science* **2003**, *299*, 377.
(36) Henderson, M. A. *Surf. Sci.* **1999**, *419*, 174.
(37) Henderson, M. A. *Surf. Sci.* **1995**, *343*, L1156.
(38) Stone, P.; Bennett, R. A.; Bowker, M. *New J. Phys.* **1999**, *1*, 1.1.
(39) Pang, C. L.; Haycock, S. A.; Raza, H.; Murray, P. W.; Thornton, G.; Gulseren, O.; James, R.; Bullett, D. W. *Phys. Rev. B* **1998**, *58*, 1586.
(40) Onishi, H.; Iwasawa, Y. *Surf. Sci.* **1994**, *313*, L783.
(41) Maksymovych, P.; Mezhenny, S.; Yates, J. T., Jr. *Chem. Phys. Lett.* **2003**, *382*, 270.
(42) Mezhenny, S.; Maksymovych, P.; Thompson, T. L.; Diwald, O.; Stahl, D.; Walck, S. D.; Yates, J. T., Jr. *Chem. Phys. Lett.* **2003**, *369*, 152.
(43) Asahi, R.; Morikawa, T.; Ohwaki, T.; Aoki, K.; Taga, Y. *Science* **2001**, *293*, 269.
(44) Diwald, O.; Thompson, T. L.; Zubkov, T.; Goralski, E. G.; Walck, S. D.; Yates, J. T., Jr. *J. Phys. Chem. B* **2004**, *108*, 6004.
(45) Batzill, M.; Morales, E. H.; Diebold, U. *Phys. Rev. Lett.* **2006**, *96*, 026103.
(46) Fleischauer, P. D.; Kan, H. K. A.; Shepard, J. R. *J. Am. Chem. Soc.* **1972**, *94*, 283.
(47) Hotsenpiller, P. A. M.; Bolt, J. D.; Farneth, W. E.; Lowekamp, J. B.; Rohrer, G. S. *J. Phys. Chem. B* **1998**, *102*, 3216.
(48) Lowekamp, J. B.; Rohrer, G. S.; Hotsenpiller, P. A. M.; Bolt, J. D.; Farneth, W. E. *J. Phys. Chem. B* **1998**, *102*, 7323.
(49) Diwald, O.; Thompson, T. L.; Goralski, E. G.; Walck, S. D.; Yates, J. T., Jr. *J. Phys. Chem. B* **2004**, *108*, 52.
(50) Chen, X.; Burda, C. *J. Phys. Chem. B* **2004**, *108*, 15446.
(51) Sato, S.; Nakamura, R.; Abe, S. *Appl. Catal. A*−*Gen.* **2005**, *284*, 131.
(52) Chen, X.; Lou, Y.-B.; Samia, A. C. S.; Burda, C.; Gole, J. L. *Adv. Funct. Mater.* **2005**, *15*, 41.
(53) Mrowetz, M.; Balcerski, W.; Colussi, A. J.; Hoffmann, M. R. *J. Phys. Chem. B* **2004**, *108*, 17269.
(54) Gole, J. L.; Stout, J. D.; Burda, C.; Lou, Y.; Chen, X. *J. Phys. Chem. B* **2004**, *108*, 1230.
(55) Di Valentin, C.; Pacchioni, G.; Selloni, A. *Phys. Rev. B* **2004**, *70*, 085116.
(56) Nakamura, R.; Tanaka, T.; Nakato, Y. *J. Phys. Chem. B* **2004**, *108*, 10617.
(57) Miyauchi, M.; Ikezawa, A.; Tobimatsu, H.; Irie, H.; Hashimoto, K. *Phys. Chem. Chem. Phys.* **2004**, *6*, 865.
(58) Lee, J. Y.; Park, J.; Cho, J. H. *Appl. Phys. Lett.* **2005**, *87*, 011904.
(59) Di Valentin, C.; Pacchioni, G.; Selloni, A.; Livraghi, S.; Giamello, E. *J. Phys. Chem. B* **2005**, *109*, 11414.
(60) Khan, S. U. M.; Al-Shahry, M.; Ingler, W. B. *Science* **2002**, *297*, 2243.
(61) Honda, K.; Fujishima, A. *Nature* **1972**, *238*, 37.
(62) Sakthivel, S.; Kisch, H. *Angew. Chem., Int. Ed.* **2003**, *42*, 4908.
(63) Tachikawa, T.; Tojo, S.; Kawai, K.; Endo, M.; Fujitsuka, M.; Ohno, T.; Nishijima, K.; Miyamoto, Z.; Majima, T. *J. Phys. Chem. B* **2004**, *108*, 19299.
(64) Nakano, Y.; Morikawa, T.; Ohwaki, T.; Taga, Y. *Appl. Phys. Lett.* **2005**, *87*, 052111.
(65) Di Valentin, C.; Pacchioni, G.; Selloni, A. *Chem. Mater.* **2005**, *17*, 6656.
(66) Thompson, T. L.; Yates, J. T., Jr. *J. Phys. Chem. B* **2005**, *109*, 18230.
(67) Dvoranova, D.; Brezova, V.; Mazur, M.; Malati, M. A. *Appl. Catal. B*−*Environ.* **2002**, *37*, 91.
(68) Martin, S. T.; Morrison, C. L.; Hoffmann, M. R. *J. Phys. Chem.* **1994**, *98*, 13695.
(69) Li, X. Y.; Yue, P. L.; Kutal, C. *New J. Chem.* **2003**, *27*, 1264.
(70) Piera, E.; Tejedor-Tejedor, M. I.; Zorn, M. E.; Anderson, M. A. *Appl. Catal. B*−*Environ.* **2003**, *46*, 671.
(71) Zhao, X. F.; Meng, X. F.; Zhang, Z. H.; Liu, L.; Jia, D. Z. *J. Inorg. Mater.* **2004**, *19*, 140.
(72) Wu, S. X.; Ma, Z.; Qin, Y. N.; He, F.; Jia, L. S.; Zhang, Y. J. *Acta Phys.*−*Chim. Sin.* **2003**, *19*, 967.
(73) Choi, W. Y.; Termin, A.; Hoffmann, M. R. *J. Phys. Chem.* **1994**, *98*, 13669.
(74) Karvinen, S.; Hirva, P.; Pakkanen, T. A. *J. Mol. Struct.*−*THEOCHEM* **2003**, *626*, 271.
(75) Choi, W. Y.; Termin, A.; Hoffmann, M. R. *Angew. Chem., Int. Ed.* **1994**, *33*, 1091.
(76) Panayotov, D.; Yates, J. T., Jr. *Chem. Phys. Lett.* **2003**, *381*, 154.
(77) Panayotov, D. A.; Yates, J. T., Jr. *Chem. Phys. Lett.* **2005**, *410*, 11.
(78) Livingston, J. D. *Electronic Properties of Engineering Materials*; Wiley: New York, 1999.
(79) Szczepankiewicz, S. H.; Colussi, A. J.; Hoffmann, M. R. *J. Phys. Chem. B* **2000**, *104*, 9842.
(80) Szczepankiewicz, S. H.; Moss, J. A.; Hoffmann, M. R. *J. Phys. Chem. B* **2002**, *106*, 2922.
(81) Yamakata, A.; Ishibashi, T.; Onishi, H. *Chem. Phys. Lett.* **2001**, *333*, 271.
(82) Rothenberger, G.; Moser, J.; Gratzel, M.; Serpone, N.; Sharma, D. K. *J. Am. Chem. Soc.* **1985**, *107*, 8054.
(83) Baraton, M. I.; Merhari, L. *Nanostruct. Mater.* **1998**, *10*, 699.
(84) Iyengar, R. D.; Codell, M. *Adv. Colloid Interface Sci.* **1972**, *3*, 365.
(85) Howe, R. F. *Adv. Colloid Interface Sci.* **1982**, *18*, 1.
(86) Howe, R. F.; Gratzel, M. *J. Phys. Chem.* **1987**, *91*, 3906.
(87) Li, S. S. *Semiconductor Physical Electronics*; Plenum Press: New York, 1993.
(88) Shockley, W.; Read Jr., W. T. *Phys. Rev.* **1952**, *87*, 835.
(89) Henderson, M. A.; Epling, W. S.; Perkins, C. L.; Peden, C. H. F.; Diebold, U. *J. Phys. Chem. B* **1999**, *103*, 5328.
(90) Lu, G. Q.; Linsebigler, A.; Yates, J. T., Jr. *J. Chem. Phys.* **1995**, *102*, 4657.
(91) Rusu, C. N.; Yates, J. T., Jr. *Langmuir* **1997**, *13*, 4311.
(92) Anpo, M.; Che, M.; Fubini, B.; Garrone, E.; Giamello, E.; Paganini, M. C. *Top. Catal.* **1999**, *8*, 189.
(93) de Lara-Castells, M. P.; Krause, J. L. *J. Chem. Phys.* **2001**, *115*, 4798.
(94) de Lara-Castells, M. P.; Krause, J. L. *Chem. Phys. Lett.* **2002**, *354*, 483.
(95) Egerton, T. A.; King, C. J. *J. Oil Colour Chem. Assoc.* **1979**, *62*, 386.
(96) Cunningham, J.; Hodnett, B. K. *J. Chem. Soc., Faraday Trans.* **1981**, *77*, 2777.
(97) Kormann, C.; Bahnemann, D. W.; Hoffmann, M. R. *Environ. Sci. Technol.* **1991**, *25*, 494.
(98) Peral, J.; Domenech, X.; Ollis, D. F. *J. Chem. Technol. Biotechnol.* **1997**, *70*, 117.
(99) D'Oleiveira, J.-C.; Al-Sayyed, G.; Pichat, P. *Environ. Sci. Technol.* **1990**, *24*, 990.
(100) Okamoto, K.; Yamamoto, Y.; Tanaka, H.; Itaya, A. *Bull. Chem. Soc. Jpn.* **1985**, *58*, 2023.
(101) Cornu, C. J. G.; Colussi, A. J.; Hoffmann, M. R. *J. Phys. Chem. B* **2001**, *105*, 1351.
(102) Cornu, C. J. G.; Colussi, A. J.; Hoffmann, M. R. *J. Phys. Chem. B* **2003**, *107*, 3156.
(103) Schwarzburg, K.; Willig, F. *Appl. Phys. Lett.* **1991**, *58*, 2520.
(104) Ho, C. T.; Bell, R. O.; Wald, F. V. *Appl. Phys. Lett.* **1977**, *31*, 463.
(105) Fabre, E.; Mautref, M.; Mircea, A. *Appl. Phys. Lett.* **1975**, *27*, 239.
(106) Ghosh, A. K.; Wakim, F. G.; Addiss, P. R. *Phys. Rev. Lett.* **1969**, *184*, 979.
(107) Hoyer, P.; Weller, H. *J. Phys. Chem.* **1995**, *99*, 14096.
(108) Nelson, J.; Haque, S. A.; Klug, D. R.; Durrant, J. R. *Phys. Rev. B* **2001**, *6320*, 205321.
(109) Xiao-e, L.; Green, A. N. M.; Haque, S. A.; Mills, A.; Durrant, J. R. *J. Photochem. Photobiol. A* **2004**, *162*, 253.
(110) Micic, O. I.; Zhang, Y. N.; Cromack, K. R.; Trifunac, A. D.; Thurnauer, M. C. *J. Phys. Chem.* **1993**, *97*, 13284.

(111) Yoshihara, T.; Katoh, R.; Furube, A.; Tamaki, Y.; Murai, M.; Hara, K.; Murata, S.; Arakawa, H.; Tachiya, M. *J. Phys. Chem. B* **2004**, *108*, 3817.
(112) Tan, T.; Beydoun, D.; Amal, R. *J. Photochem. Photobiol. A* **2003**, *159*, 273.
(113) Du, Y. K.; Rabani, J. *J. Phys. Chem. B* **2003**, *107*, 11970.
(114) Nakamura, R.; Nakato, Y. *J. Am. Chem. Soc.* **2004**, *126*, 1290.
(115) Goto, H.; Hanada, Y.; Ohno, T.; Matsumura, M. *J. Catal.* **2004**, *225*, 223.
(116) Shkrob, I. A.; Sauer, M. C. *J. Phys. Chem. B* **2004**, *108*, 12497.
(117) Lana-Villarreal, T.; Bisquert, J.; Mora-Seró, I.; Salvador, P. *J. Phys. Chem. B* **2005**, *109*, 10355.
(118) de Lara-Castells, M. P.; Krause, J. L. *J. Chem. Phys.* **2003**, *118*, 5098.
(119) Henderson, M. A.; Epling, W. S.; Peden, C. H. F.; Perkins, C. L. *J. Phys. Chem. B* **2003**, *107*, 534.
(120) Berger, T.; Sterrer, M.; Diwald, O.; Knozinger, E. *ChemPhysChem* **2005**, *6*, 2104.
(121) Lu, G. Q.; Linsebigler, A.; Yates, J. T., Jr. *J. Chem. Phys.* **1995**, *102*, 3005.
(122) Perkins, C. L.; Henderson, M. A. *J. Phys. Chem. B* **2001**, *105*, 3856.
(123) Thompson, T. L.; Yates, J. T., Jr. *J. Phys. Chem. B* **2006**, *110*, 7431.
(124) Kopelman, R. *J. Stat. Phys.* **1986**, *42*, 185.
(125) Kopelman, R. *Science* **1988**, *241*, 1620.
(126) Kopelman, R. In *The Fractal Approach to Heterogeneous Chemistry: Surfaces Colloids and Polymers*; Avnir, D., Ed.; Wiley: New York, 1989.
(127) Vijay, A.; Mills, G.; Metiu, H. *J. Chem. Phys.* **2003**, *118*, 6536.
(128) Yamakata, A.; Ishibashi, T.; Onishi, H. *J. Phys. Chem. B* **2001**, *105*, 7258.
(129) Panayotov, D. A.; Yates, J. T. *Chem. Phys. Lett.* **2004**, *399*, 300.
(130) Zubkov, T.; Stahl, D.; Thompson, T. L.; Panayotov, D.; Diwald, O.; Yates, J. T., Jr. *J. Phys. Chem. B* **2005**, *109*, 15454.
(131) Neumann, A. W.; Good, R. J. In *Surface and Colloid Science, Experimental Methods*; Good, R. J., Stromberg, R. R., Eds.; Plenum: New York, 1979; Vol. II.
(132) Adamson, A.; Gast, A. *Physical Chemistry of Surfaces*; Wiley-Interscience: New York, 1997.
(133) Sun, R. D.; Nakajima, A.; Fujishima, A.; Watanabe, T.; Hashimoto, K. *J. Phys. Chem. B* **2001**, *105*, 1984.
(134) Miyauchi, M.; Nakajima, A.; Fujishima, A.; Hashimoto, K.; Watanabe, T. *Chem. Mater.* **2000**, *12*, 3.
(135) Nakajima, A.; Koizumi, S.; Watanabe, T.; Hashimoto, K. *J. Photochem. Photobiol. A* **2001**, *146*, 129.
(136) Sakai, N.; Fujishima, A.; Watanabe, T.; Hashimoto, K. *J. Phys. Chem. B* **2001**, *105*, 3023.
(137) Sakai, N.; Fujishima, A.; Watanabe, T.; Hashimoto, K. *J. Phys. Chem. B* **2003**, *107*, 1028.
(138) Nakajima, A.; Koizumi, S.; Watanabe, T.; Hashimoto, K. *Langmuir* **2000**, *16*, 7048.
(139) Miyauchi, M.; Kieda, N.; Hishita, S.; Mitsuhashi, T.; Nakajima, A.; Watanabe, T.; Hashimoto, K. *Surf. Sci.* **2002**, *511*, 401.
(140) Sakai, N.; Wang, R.; Fujishima, A.; Watanabe, T.; Hashimoto, K. *Langmuir* **1998**, *14*, 5918.
(141) Wang, R.; Sakai, N.; Fujishima, A.; Watanabe, T.; Hashimoto, K. *J. Phys. Chem. B* **1999**, *103*, 2188.
(142) Bouzoubaa, A.; Markovits, A.; Calatayud, M.; Minot, C. *Surf. Sci.* **2005**, *583*, 107.
(143) White, J. M.; Szanyi, J.; Henderson, M. A. *J. Phys. Chem. B* **2003**, *107*, 9029.
(144) Gao, Y. F.; Masuda, Y.; Koumoto, K. *Langmuir* **2004**, *20*, 3188.
(145) Wang, C. Y.; Groenzin, H.; Shultz, M. J. *Langmuir* **2003**, *19*, 7330.
(146) Nakamura, M.; Makino, K.; Sirghi, L.; Aoki, T.; Hatanaka, Y. *Surf. Coat. Technol.* **2003**, *169*, 699.

CR050172K